THEORETICAL AND EXPERIMENTAL INVESTIGATIONS OF ARTERIAL PULSE WAVE VELOCITY (PWV)

By

Mohammad Yavarimanesh

A DISSERTATION

Submitted to
Michigan State University
in partial fulfillment of the requirements
for the degree of

Electrical Engineering- Doctor of Philosophy

2021

ABSTRACT

THEORETICAL AND EXPERIMENTAL INVESTIGATIONS OF ARTERIAL PULSE WAVE VELOCITY (PWV)

By

Mohammad Yavarimanesh

Pulse transit time (PTT) is the time delay for the energy wave to travel between two sites in the arteries. (The energy wave can be visualized as acute dilation of the arterial wall and usually moves much faster than blood.) PTT in the form of pulse wave velocity (PWV = D/PTT, where D is the distance between the two sites) has proven to be a marker of arterial stiffness and a major cardiovascular risk factor based on a large body of epidemiological data. The Bramwell-Hill (BH) equation relates arterial stiffness and radius to PWV. Arterial stiffness positively relates to blood pressure (BP); thus, many have pursued BP monitoring via PWV. We investigated PWV from theoretical, experimental, and application prospective.

In the first theory study, we investigated the 100-year Bramwell-Hill equation, which relates PWV to BP and thus represents a basis for cuff-less BP monitoring. However, it has long been known that this equation underestimates PWV in a BP-dependent manner. We developed a new equation that accounts for spatial changes in arterial cross-sectional area. This new equation largely corrected this well-known underestimation and predicted PWV better based on experimental data in the literature.

In the second experimental study, we examined the most popular PTT (finger PTT). We hypothesize that whole body PTT could be better than finger PTT due to less smooth muscle contraction. We collected data from 32 participants in a near supine position. We placed sensors including electrodes on the chest for an ECG waveform, clips on the ear, finger, and toe for photo-plethysmography (PPG) waveforms, and a cuff on the arm for auscultation BP. We recorded the

waveforms and referenced BP before and after mental arithmetic, a cold pressor test, slow breathing, and nitroglycerin. Conventional PTTs were assessed as markers of BP in human subjects undergoing a battery of interventions to change BP. This experimental study concludes that PTTs through the whole body rather than the arm show the best BP change tracking ability.

Thirdly, we repeated the previous study for seven subjects in three sessions one year apart to see how much PTTs and other PPG waveform feature models change after one year. While it is known that the PTTs calibration models must be updated periodically to account for aging effects, data on the time period required for these "cuff re-calibrations" are scant. Our experimental finding suggests that the PTTs model through the whole body could hold up after one year, and calibration may occur every year, which is reasonably practical.

Finally, because of the inverse relation of PWV and arterial radius in the BH equation, we investigated innovative applications for PTT and other physiology-inspired features of carotid and femoral waveform for screening and surveillance of aortic abdominal aneurysm diameter. We hypothesized that arterial waveform features such as PTT constitute a non-imaging solution for the aneurysm size of the aorta. The features detected AAA with 72-80% accuracy.

To my parents, my sister and Nilu.

ACKNOWLEDGMENTS

I had a great time with my advisor Prof. Mukkamala. It was impossible to complete my Ph. D. without him. He truly guided me not only in science but also in my life. He is really a great role model for me.

Also, I would like to thank all my committee members (Prof. Subir Biswas, Prof. Selin Aviyente, and Prof. Seungik Baek) for their valuable inputs during my presentations. Furthermore, I would like to thank all my labmates (Anand Chandrasekhar and Keerthana Natrajan) for all their help and support on my research.

Also, I like to say special thanks to my family and friends for their constructive support and help throughout my life. Last but not least, I thank my life coach, Molana, for his lifesaving advices and the Almighty for everything that happened in my life.

TABLE OF CONTENTS

LIST OF TABLES

LIST OF FIGURES

Chapter 1. Introduction

1.1 PWV/PTT Definition

PTT (Pulse Transit Time) is the time delay for the energy wave to travel between two sites in the arteries (Figure 1-1A). (The energy wave can be visualized as acute dilation of the arterial wall and usually moves much faster than blood.) PTT is inversely related to PWV (Pulse Wave Velocity) (PWV = D/PTT, D is the distance between the two sites).

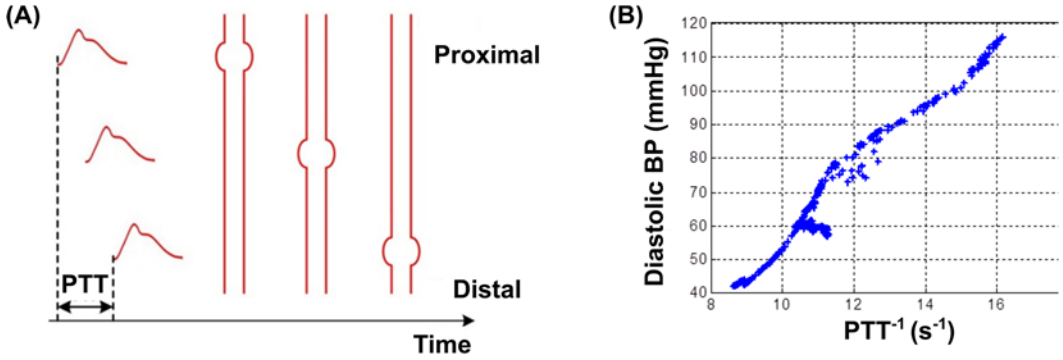

Figure 1-1 PTT definition and relation to blood pressure.

1.2 Conventional Ways to Measure PWV/PTT

PTT can be estimated simply from the relative timing between proximal and distal waveforms indicative of the arterial pulse. Conventionally, PTT is determined by (1) measuring (a) ECG and ear, finger, or toe PPG waveforms or (b) two of these PPG waveforms and (2) detecting the time delay between the waveforms.

1.3 PWV/PTT Application

PTT represents a potential approach for improved BP (Blood Pressure) monitoring. According to the Bramwell-Hill equation, PTT varies with AC (Arterial Compliance, a derivative of arterial volume with respect to pressure). Indeed, PTT in the form of PWV has proven to be a marker of

arterial stiffness and a major cardiovascular risk factor based on a large body of epidemiological data.

It has long been known that PTT also shows a tight relationship with BP (figure 1-1B). Hence, PTT could permit non-invasive, automatic, and cuff-less BP monitoring for durations up to perhaps a few years at a time. As a result, BP monitoring via PTT has captured the interest of many.

1.4 PWV/PTT Challenges

The first challenge is about the theory basis. While the Bramwell-Hill (BH) equation is widely used to relate PWV to arterial stiffness and B, it has long been known that this equation underestimates PWV in a BP-dependent manner.

The second challenge is that there is no study in which conventional PTTs are evaluated as markers of BP changes under a battery of nontrivial BP-varying interventions in a relatively large number of normotensive and hypertensive humans.

The third challenge is about the calibration curve, which related PTTs in the unit of sec to BP in mmHg. While it is known that the calibration curve must be updated periodically to account for aging effects, data on the time period required for these "cuff re-calibrations" are scant.

The study objective of this research is to address these challenges and find another potential application for PTTs.

1.5 Organization

This thesis is organized as follows. Chapter 2 introduce new formula related PWV to BP by relaxing the central assumption of the Bramwell-Hill equation. Chapter 3 reports comparing the cPTTs as markers of BP changes under a battery of nontrivial BP-varying interventions in a relatively large number of normotensive and hypertensive humans. Chapter 4 shows the results of

repeating the chapter 3 study for two years to see how much calibration curves change after one year of aging. Chapter 5 suggests innovative applications for the PWVs for screening and surveillance of AAA (Aortic Abdominal Aneurysms). In the end, chapter 6 discuss the future works.

Chapter 2. A Superior Equation for Relating Pulse Wave Velocity to Arterial Stiffness and Blood Pressure

2.1 Introduction

The Bramwell-Hill (BH) equation for indicating that pulse wave velocity (PWV, v) increases with arterial stiffening is century-old [1] but still widely used [2], [3]. This equation, which was also published in German by Frank at about the same time and has even earlier origins [4], is given as follows:

$$v_{BH} = \sqrt{\frac{A}{\rho}\frac{dP}{dA}}, \tag{2.1}$$

where A is the cross-sectional area of the artery, ρ is the density of blood therein, P is the blood pressure (BP), and dA/dP is the arterial compliance. The ratio of arterial compliance to area denotes the distensibility, which is an inverse metric of arterial stiffness. Arterial distensibility decreases slowly over time due to aging and as BP increases due to the nonlinear properties of the arterial wall [2], [5], [6]. In this way, the BH equation also provides a direct relationship between PWV and BP. Recent studies have captured interest by proposing to leverage this PWV-BP relationship in conjunction with stretchable skin sensors for detecting PWV via the arterial pulse time delay to track BP changes seamlessly without an inflatable cuff [7], [8].

Yet, it has long been known that the BH equation underestimates PWV [1,9–21]. In fact, early investigators proposed empirical scale factors of 1.1-1.7 to correct the underestimation of PWV in the aorta [9], [13]–[16], [21]. They also presented plots like Figure 2-1A to show that such a correction (solid line) would still misestimate PWV (data points) in the low BP range [9]. Hence, their conclusion was that an accurate correction of the BH equation would depend on BP.

The early investigators explained that the reason for the PWV underestimation is that the BH

equation only considers the elastic nature of the arterial wall and thus ignores its viscous component [1], [9], [13]–[15], [21]. A viscoelastic artery would dilate under distending BP in a dynamic manner such that the distensibility appears as a lowpass function of frequency. This explanation was based on their own experiments wherein they measured the aortic distensibility for predicting PWV via "slow stretch curves" (which corresponds to the static distensibility) but measured PWV via the time delay between the sharp onsets of upstroke or "feet" of proximal and distal aortic pulses (which corresponds to a lower apparent distensibility at the higher frequencies).

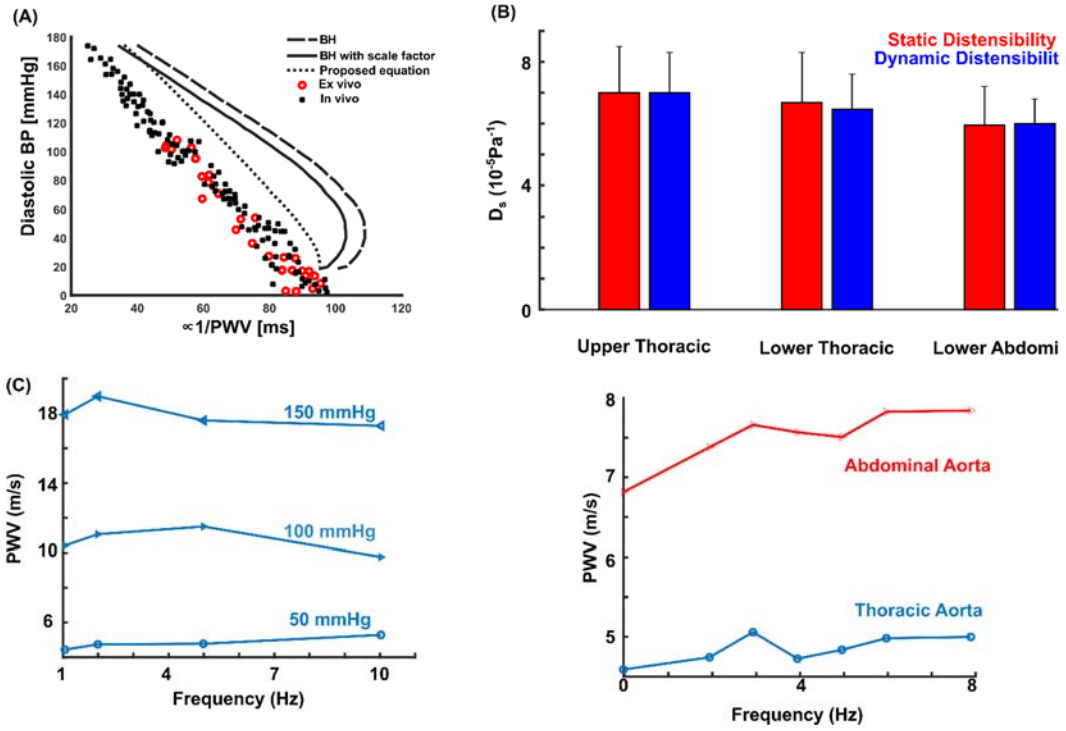

Figure 2-1 Early investigator explanation for underestimation.
(A) Early aortic pulse wave velocity (PWV) data showing measurement (data points) and predictions as a function of blood pressure (BP) by the Bramwell-Hill (BH) equation with (dashed line) and without (solid line) an empirical scale factor correction (adapted from [9]). The improved PWV prediction of the proposed equation (dotted line) is also included. Later arterial wall viscoelasticity data showing that (B) aortic distensibility or PWV as predicted from aortic distensibility via the BH equation is not strongly dependent on frequency (adapted from [17], [22]) and (C) the BP level only modestly impacts the dependency of arterial distensibility on frequency (adapted from [22]).

However, subsequent researchers found that the aorta exhibits only minor viscoelastic behaviors [17], [22]–[24]. For example, the data shown in Figure 2-1B indicates that aortic PWV predicted with the apparent distensibility at high frequency may be no more than 10% higher than the PWV predicted with the static distensibility [17,22–23]. This difference is less than what would be needed for the proposed 1.1-1.7 empirical scale factor corrections. Later investigators also reported that arterial viscoelastic effects are similar at different BP levels, as illustrated in Figure 2-1C [22], [24]. Hence, accounting for viscoelasticity may not yield a

correction to the BH equation that is substantively dependent on BP. Furthermore, and perhaps most importantly, early to recent investigators have consistently shown that inserting the apparent rather than static distensibility into the BH equation still results in significant underestimation of PWV (see Table below).

Our hypothesis is that the BH equation underestimates PWV as a result of neglecting spatial changes in A. This hypothesis is based on two considerations. First, including such changes would increase the net force acting on the wave so as to increase the predicted PWV. Second, since distensibility and thus A changes are sensitive functions of BP, the predicted PWV increase would be dependent on BP. Here, we derive an equation that incorporates spatial changes in A and show that this equation can improve PWV prediction accuracy using experimental data (see, e.g., dotted line in Figure 2-1A). The proposed equation may offer a superior means for quantifying arterial stiffness and for calibrating potential cuff-less systems to yield BP in units of mmHg from PWV measurements in units of m/s.

2.2 Proposed PWV Equation

We begin by assuming that an artery can be represented as a long cylindrical tube wherein the tube wall is composed of homogenous, elastic material; blood is incompressible; and flow is inviscid and in the axial direction with uniform velocity profile. These assumptions are most tenable for the aorta [2] and are likewise made when deriving the BH equation. We then imagine wave propagation in such an artery as presented in Movie S1. Figure 2-2 shows successive snapshots of a portion of the artery in this animation wherein the geometry of the wave propagating in the artery has been simplified (from spherical to cylindrical) for mathematical convenience. At some time $t = t_i$ (top panel of figure), the arterial segment to the left has larger A, P, and blood volume flow rate (Q) by Δ amounts than the two segments to the right as well as

other such segments that are not shown. After a Δt time interval (bottom panel), this disturbance has traveled over a Δx space interval to the middle arterial segment. The uniform movement of the disturbance is also illustrated at the midpoint of the two time instances (center panel). We derive an equation for the speed of this movement by employing a fixed control volume approach as follows.

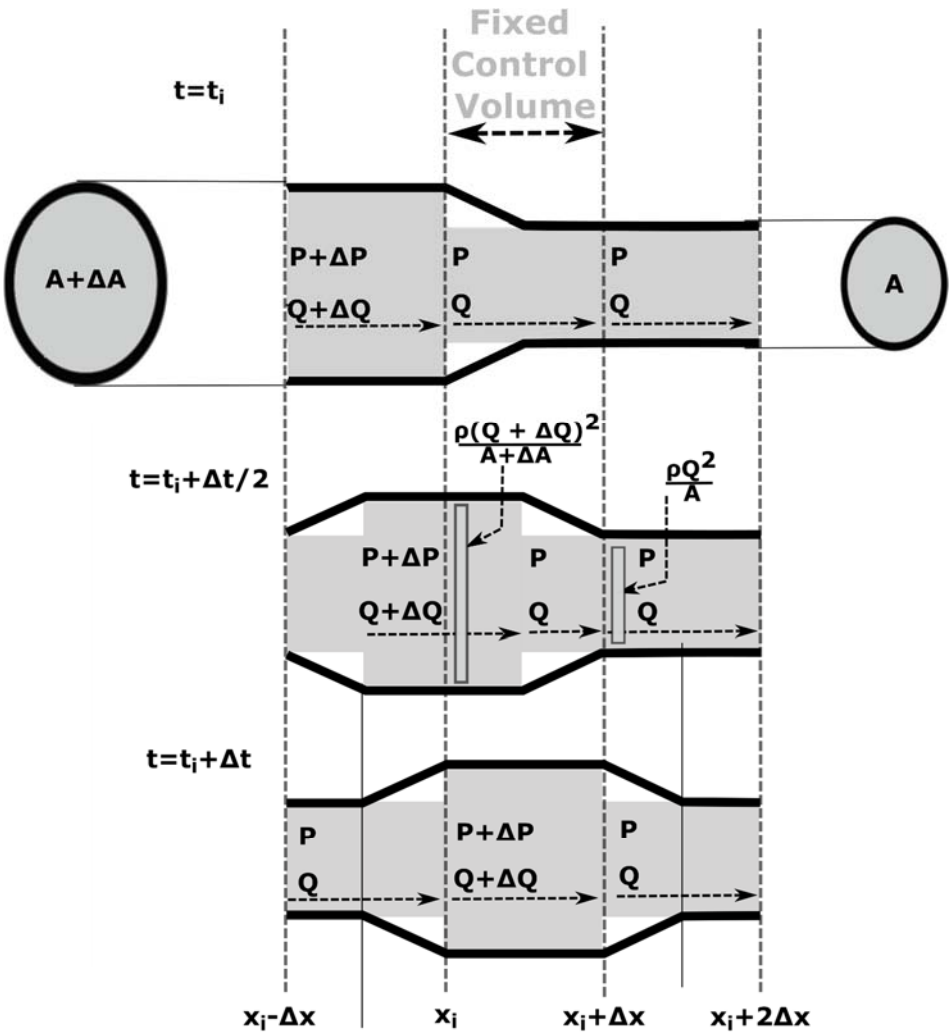

Figure 2-2 Model of arterial wave propagation for deriving the proposed PWV equation.

The underlying assumptions are the same as the standard BH equation. The key difference is that spatial changes in arterial cross-sectional area (A) are assumed to be an important factor (see Movie S1). P is blood pressure; Q, blood volume flow rate; x, space; t, time; Δ, incremental amount; and ρ, blood density. See text for detailed explanation.

We first apply conservation of mass to our model. The net ΔQ into the control volume over the Δt time interval (top panel of figure) is balanced by the ΔA increase over the Δx space interval of the control volume (bottom panel) to yield the following equation:

$$\Delta Q \cdot \Delta t = \Delta A \cdot \Delta x. \tag{2.2}$$

To transform this equation into conventional partial derivative notation, it can be inferred from the figure that $\partial/\partial x = -\Delta/\Delta x$ and $\partial/\partial t = \Delta/\Delta t$. Hence, the standard equation for conservation of mass results as follows:

$$-\frac{\partial Q}{\partial x} = \frac{\partial A}{\partial t}. \tag{2.3}$$

We then apply conservation of momentum to the model by invoking the following one-dimensional Reynold's transport theorem:

$$F = \frac{d}{dt}\int_{C.V.} \frac{\rho Q}{A}\partial\Omega + (\rho Q^2/A)_{out} - (\rho Q^2/A)_{in}, \tag{2.4}$$

where F is the net, right directional force acting on the control volume ($C.V.$), the first term to the right of the equality is the time rate of change of momentum within the control volume, and the last two terms are the flux of momentum passing out and into the control surfaces. We assume that the control volume here is the fluid shown in the middle arterial segment at the midpoint time (center panel of figure), as it may be representative of the entire Δt time interval. To specify F, note that the fluid disturbance is concentrated and thus induces transient displacement of the arterial wall surface from the fluid at its lateral edges [25] . This assumption of momentary tent-like arterial distension represents an analogy between mechanical deformation under solid and liquid impact [26]. Due to the key assumption, the wall does not exert any net x-direction force on the control volume, and the disturbance may be viewed as both fluid and the expanded region

that move quickly in concert at the PWV (recall Movie S1). This x-direction movement may be faster than any y-direction movement of blood into the expanded region due to gravity. For example, assuming a normal PWV of 5 m/s [5] and initial blood velocity of zero in the y-direction, the x-direction distance traveled by the wave (d in meters) relative to the y-direction distance traveled by blood due to gravity over some time interval is $5.1/d$. Hence, the relative distance increases with decreasing d.

The following equation for the model then results:

$$(P+\Delta P)\,(A+\Delta A)-PA=\frac{d}{dt}\left(\frac{\rho(Q+\Delta Q)}{(A+\Delta A)}(A+\Delta A)\frac{\Delta x}{2}+\frac{\rho Q}{A}A\frac{\Delta x}{2}\right)+\frac{\rho Q^2}{A}-\frac{\rho(Q+\Delta Q)^2}{A+\Delta A}. \tag{2.5}$$

Neglecting terms that are relatively small (either quadratic or because $P \gg \rho Q^2/A^2$, i.e., BP is much larger than twice the kinetic energy in arteries [27]) and using partial derivative notation yields the following equation for conservation of momentum:

$$-A\frac{\partial P}{\partial x}-\boldsymbol{P\frac{\partial A}{\partial x}}=\rho\frac{\partial Q}{\partial t}. \tag{2.6}$$

The bold term in this equation is an extra term that does not appear in the standard conservation of momentum equation used to derive the BH equation. Conventionally, this term is neglected by either assuming (i) the relative change in A is small compared to the relative change in P (i.e., $\frac{P}{PA}\frac{\partial A}{\partial x} \ll \frac{A}{PA}\frac{\partial P}{\partial x}$) [28] or (ii) the artery instantaneously conforms to the shape of the fluid disturbance such that the fluid in the ΔA area exerts a rightward force on the wall that is balanced by leftward axial wall stress (i.e., $P\partial A$ is negated by equal and opposite axial wall force) [29].

We next substitute BP-dependent arterial compliance ($dA/dP = C(P)$) into Eqs. (2-3) and (2-6) to yield the following coupled set of nonlinear, partial differential equations:

$$\frac{\partial Q}{\partial x}=-C(P)\frac{\partial P}{\partial t} \tag{2.7}$$

$$\frac{\partial P}{\partial x} = -\frac{\rho}{A+\boldsymbol{PC(P)}}\frac{\partial Q}{\partial t}. \tag{2.8}$$

Again, the bold term in Eq. (2-8) is extra relative to the standard equations. Note that another difference between Eqs. (2-7) and (2-8) and the standard equations is that arterial compliance in the latter is assumed constant (i.e., C) rather than BP-dependent (i.e., $C(P)$). However, as indicated below, relaxing the constant arterial compliance assumption has no effect on the PWV equation.

To solve Eqs. (2-7) and (2-8) and thereby yield the final equation, we state, prove, and then invoke the following theorem.

Theorem: Suppose a coupled set of nonlinear, partial differential equations are of the following form:

$$\frac{\partial Q}{\partial x} = -g(P)\frac{\partial P}{\partial t} \tag{2.9}$$

$$\frac{\partial P}{\partial x} = -h(P)\frac{\partial Q}{\partial t}, \tag{2.10}$$

where $g(\cdot)$ and $h(\cdot)$ are any positive-valued and differentiable functions. By generalizing the well-known solution to the standard equations, the solution for P in Eqs. (2-9) and (2-10) is a wave ($f(\cdot)$) traveling at a speed of $(h(P)g(P))^{-1/2}$ as follows:

$$P = f\left(x \pm \sqrt{\frac{1}{h(P)g(P)}}t\right). \tag{2.11}$$

Proof: We first define a new variable s as follows:

$$s = x \pm \sqrt{\frac{1}{h(P)g(P)}}t. \tag{2.12}$$

We then use Eq. (2-12) to determine the partial derivatives of the presumptive solution P in Eq. (2-11) with respect to x and t as follows:

$$\frac{\partial P}{\partial x}=\frac{\partial P}{\partial s}\ \frac{\partial s}{\partial x}=\frac{\frac{\partial P}{\partial s}}{1\pm\frac{1}{2}\left(h(P)g(P)\right)^{-\frac{3}{2}}\left(\frac{dh(P)}{dP}g(P)+h(P)\frac{dg(P)}{dP}\right)t\frac{\partial P}{\partial s}} \tag{2.13}$$

$$\frac{\partial P}{\partial t}=\frac{\partial P}{\partial s}\ \frac{\partial s}{\partial t}=\frac{-\left(h(P)g(P)\right)^{-\frac{1}{2}}\frac{\partial P}{\partial s}}{1\pm\frac{1}{2}\left(h(P)g(P)\right)^{-\frac{3}{2}}\left(\frac{dh(P)}{dP}g(P)+h(P)\frac{dg(P)}{dP}\right)t\frac{\partial P}{\partial s}}. \tag{2.14}$$

We next combine Eqs. (2-13) and (2-14) to yield the following equation:

$$\frac{\partial P}{\partial t}=-\sqrt{\frac{1}{h(P)g(P)}}\ \frac{\partial P}{\partial x}. \tag{2.15}$$

We thereafter substitute Eq. (2-15) into Eqs. (2-9) and (2-10) to yield the following equations:

$$\frac{\partial Q}{\partial x}=\sqrt{\frac{g(P)}{h(P)}}\ \frac{\partial P}{\partial x} \tag{2.16}$$

$$-\sqrt{h(P)g(P)}\ \frac{\partial P}{\partial t}=-h(P)\frac{\partial Q}{\partial t}. \tag{2.17}$$

We complete the proof by manipulating Eqs. (2-16) and (2-17) to yield the same equation as follows:

$$\frac{\partial P}{\partial Q}=\sqrt{\frac{h(P)}{g(P)}}. \tag{2.18}$$

Note that the solution for Q may be obtained by integrating Eq. (2-18) while invoking Eq. (2-11) and is therefore a wave likewise traveling at speed of $(h(P)g(P))^{-1/2}$.

We finally apply the theorem to the governing partial differential equations of the model (Eqs. (2-7) and (2-8)) with $g(P)=C(P)=\frac{dA}{dP}$ and $h(P)=\frac{\rho}{A+PC(P)}$ to arrive at the proposed PWV equation as follows:

$$v=\sqrt{\frac{A(P)+PC(P)}{\rho C(P)}}\ \rightarrow\ v^2=v_{BH}^2+\frac{P}{\rho}. \tag{2.19}$$

Note that application of the theorem to the standard equations (i.e., $g(P) = C = \frac{dA}{dP}$ and $h(P) = \frac{\rho}{A}$) would result in the BH equation (see Eq. (2-1)). As can be seen, the proposed equation predicts higher PWV than the BH equation by a BP-dependent amount and reduces to the BH equation when $PC(P) \ll A(P) \rightarrow \frac{dA}{A} \ll \frac{dP}{P}$. This condition becomes more valid with increasing arterial stiffness, which occurs with rising BP and age. A finer point is that P in Eq. (2-19) represents transmural pressure when it is an argument of A or C but internal pressure when it is not.

2.3 Equation Validation

To validate the proposed PWV equation, we leverage a wealth of experimental data from previous studies [9]–[12], [17]–[20]. We include those studies for which (i) PWV was measured in the *in vivo* or *ex vivo* healthy aorta or a tube and (ii) the apparent distensibility of the same vessel was measured for predicting PWV as the square root of its reciprocal according to the BH equation (see Eq. (2-1)). We did not exclude any such studies that we found in the literature. PWV was always measured in the horizontal vessel under pulsatile excitation at the level of diastolic BP via the classical foot-to-foot time delay between proximal and distal pressure or vessel cross-sectional area waveforms [2], [5]. In the *ex vivo* and tube studies, fluid pressure and area waveforms were directly measured, and apparent distensibility was computed from these measurements near the diastolic pressure (e.g., slope of the line relating the initial area to pressure data points within a pulse normalized by the diastolic area). In the *in vivo* studies, BP was either invasively measured in the aorta with a catheter, non-invasively measured in the brachial artery via a cuff device, or indirectly estimated in the aorta using an arm cuff device, while area was typically measured at one or more aortic sites via imaging. Apparent

distensibility was then computed as $\frac{A_s - A_d}{A_d(P_s - P_d)}$, where s and d denote systolic and diastolic and each term may represent temporal and/or spatial averages. Note that potential sources of error for this computation include decreasing distensibility with increasing BP as the cardiac cycle progresses, residual viscoelastic effects, and pulse pressure ($P_s - P_d$) amplification for brachial BP measurements. However, the first two sources of error may have been mitigated by considering only the healthy aorta, and the net effect of these errors may be underestimation of apparent distensibility anyhow (which would increase the predicted PWV). We estimate PWV via the proposed equation here from the PWV estimate of the BH equation and diastolic BP (see right of arrow in Eq. (2-19)).

The Table summarizes comparisons between the proposed and BH equations in predicting the PWV measurements from the previous studies. The studies are listed in descending order of quality of data. As expected, the BH equation has good predictive value but consistently underestimates the PWV measurements (mean error of -1.2 m/s or -16% relative to the mean of PWV). The proposed equation always improves the PWV predictions and mitigates the underestimation by 75% (mean error of -0.3 m/s with similar SEs). Figure 2-1A likewise shows that the proposed equation can largely correct and thereby explain the BP-dependent PWV underestimation by the BH equation reported in early studies. The remaining underestimation of PWV by the proposed equation could be due in part to neglecting the smaller terms in the governing momentum equation (see Eqs. (2-5) and (2-6)).

Table 2-1. Comparisons between Proposed and Bramwell-Hill (BH) Equations in Predicting Pulse Wave Velocity (PWV) Measurements in the Literature.

Ref.	Vessel	Diastolic BP (mmHg)	PWV (m/s)			Method to Measure Apparent Distensibility for Predicting PWV
			Measured	Proposed Equation	BH Equation	
[17]	*ex vivo* aorta (N=14 per 3 sections)	75 (measured)	4.6±0.1	5.0±0.1	3.9±0.1	$C(P_d)/A_d$ (distensibility near diastolic BP) P – fluid pressure sensor A – ultrasonic crystals at section midpoint
[17]	tube (N=13)	75 (measured)	20.6±2.7	19.6±2.6	19.2±2.7	$C(P_d)/A_d$ (distensibility near diastolic BP) P – fluid pressure sensor A – ultrasonic crystals at tube midpoint
[9]	tube (M=7)	50 (measured)	8.4±0.6	7.8±0.4	7.3±0.4	$C(P_d)/A_d$ (distensibility near diastolic BP) Terms computed via dynamic stress-strain testing of tube material
[18]	*in vivo* As-Ab aorta (M=53,762)	54 (measurement average)	4.6±0.1	4.9±0.1	4.2±0.1	$(A_s - A_d)/(A_d(P_s - P_d))$ (distensibility over pulse pressure) P – aortic BP catheter A – As and De aorta imaging
[19]	*in vivo* As-Ab aorta (N=40)	85 (measurement average)	6.1±1.8	4.9±1.8	3.7±1.8	$(A_s - A_d)/(A_d(P_s - P_d))$ (distensibility over pulse pressure) P – indirect aortic cuff BP A – As, De, and Ab aorta imaging
[12]	*in vivo* As-De aorta (N=17)	76 (measurement average)	7.1±0.3	7.1±0.3	6.5±0.4	$(A_s - A_d)/(A_d(P_s - P_d))$ (distensibility over pulse pressure) P – aortic BP catheter A – De aorta imaging
[20]	*in vivo* As-Ab aorta (N=141)	84 (measurement average)	6.7±1.0	6.6±1.0	5.7±1.0	$(A_s - A_d)/(A_d(P_s - P_d))$ (distensibility over pulse pressure) P – brachial cuff BP A – As, De, and Ab aorta imaging
[10]	*in vivo* As-Ab aorta (N=22)	76 (measurement average)	4.8±0.8	4.8±0.8	3.7±0.8	$(A_s - A_d)/(A_d(P_s - P_d))$ (distensibility over pulse pressure) P – brachial cuff BP A – As, De, and Ab aorta imaging
[11]	*in vivo* As-De aorta (N=126)	80 (measurement average)	6.1±3.0	4.7±0.8	3.4±0.8	$(A_s - A_d)/(A_d(P_s - P_d))$ (distensibility over pulse pressure) P – brachial cuff BP A – As and De aorta imaging
Mean (SE) of Error (m/s)			-	**-0.3 (0.1)**	**-1.2 (0.1)**	-

Table 2-1 (cont'd)

PWV was measured via the foot-to-foot time delay between proximal and distal pulses, which corresponds to diastolic BP; PWV was predicted via the BH equation from the apparent distensibility measurement of the same vessel (Eq. (1)); and PWV was predicted via the proposed equation from the BH equation prediction and diastolic BP (Eq. (19)). The studies are listed in descending order of quality of data.

Values are mean±SE. N is number of subjects; M, number of measurements; As, ascending; Ab, abdominal; De, descending; P, blood pressure (BP); A, vessel cross-sectional area; d and s, diastolic and systolic; and $C(P_d)$, slope of $A - P$ data pairs near diastolic BP.

2.4 Discussion

The BH equation has been invoked for decades to directly relate PWV to arterial stiffness and BP. However, experimental data from early [1], [9], [13]–[16], [21] to recent studies [10]–[12], [17]–[20] have repeatedly indicated that the famous equation underestimates PWV. This underestimation was a focus of early studies [1], [9], [13]–[16], [21] but may have been overlooked with time.

The original thinking was that the BH equation underestimates PWV due to the assumption that the arterial wall is purely elastic as opposed to viscoelastic. However, the substantial, BP-dependent underestimation of aortic PWV reported in early studies (see Figure 2-1A) cannot be explained by the minor, BP-independent arterial viscoelastic behaviors observed in later studies (see Figs. 1BC). Perhaps more convincingly, the PWV underestimation is evident even after viscoelastic effects have been taken into account (see Table).

So, why then does the BH equation underestimate PWV? It cannot be that this equation ignores viscid blood flow, as such frictional force would act in the opposite direction of wave travel to further reduce PWV. It also cannot be that the equation predicts the wave speed relative to the blood velocity (e.g., the speed of the movement of ΔQ relative to the value of Q/A in Figure 2-2), whereas measured PWV is the sum of wave speed and blood velocity. The reason is that, while the average blood velocity in the aorta is about 0.5 m/s [27], the blood velocity at the feet of arterial pulses from which PWV is detected is nearly zero [5].

A possible answer is that the BH equation underestimates PWV by virtue of disregarding changes in arterial cross-sectional area (A). This assumption may have been dismissed in the past for two reasons. First, the assumption is subtle in the sense that the BH equation states that PWV is a function of A changes (see Eq. (2-1)). Hence, the BH equation does not ignore A changes altogether but rather neglects only the spatial changes in A in the equation of motion while accounting for the temporal changes in A in the equation of continuity. Second, it may be easy to assume that the arterial wall deforms instantly to the shape of the disturbance such that the fluid pressure exerted on the extra area (see ΔA in middle panel of Figure 2-2) is offset by axial wall stress that keeps the artery from breaking apart (see, e.g., Figure 3.8 in [29]). In this case, spatial changes in A would not impact the net fluid force acting on the wave. Also note that by disregarding these changes, while assuming constant arterial compliance ($\frac{dA}{dP} = C$), a standard analytical solution for PWV exists.

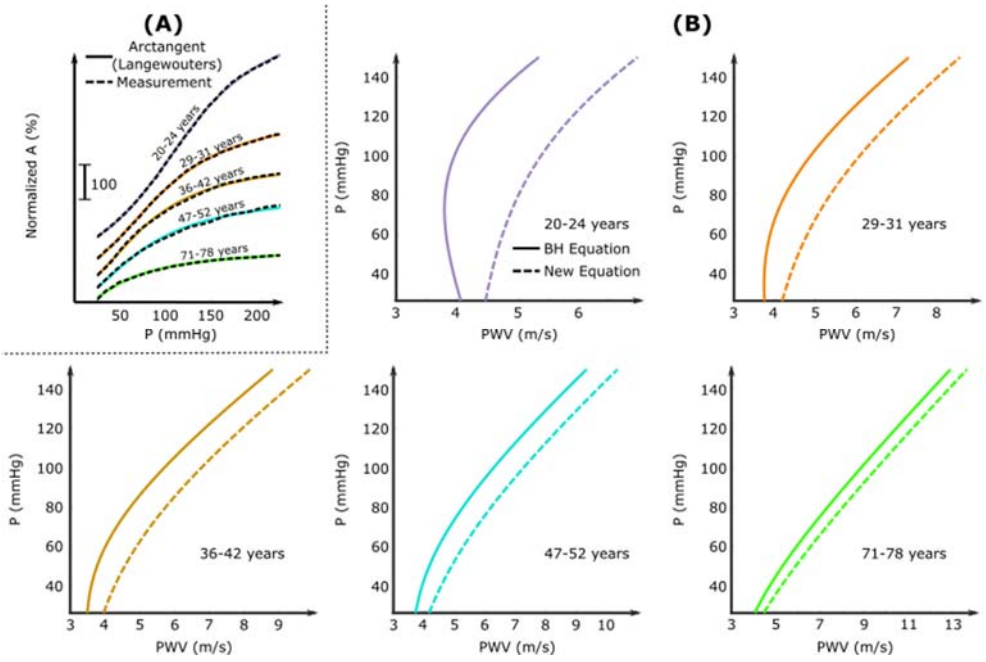

Figure 2-3 PWV and BP relation for different age groups

(A) Least squares fits of arctangent (Langewouters) $A(P)$ model of the human aorta (Eq. (20)) to independent $A-P$ measurements from ex vivo human aortas for different age groups [14]. (B) Corresponding $P-$PWV relationships resulting from substituting the model $A(P)$ fits in (A) into the proposed PWV equation (Figure 2-2) and the BH equation. The P-PWV plots are restricted to the physiologic range of diastolic BP to clearly highlight the differences.

By making an analogy between material deformation under solid and liquid impact [26], we envisioned wave propagation as a fast-moving fluid disturbance that induces tent-like arterial distension such that counter axial wall stress is not generated (see Movie S1). In this case, spatial changes in A do increase the fluid force in the direction of wave travel to augment PWV. Moreover, since BP is a major determinant of distensibility and thus A changes, the PWV increase would be dependent on BP. We thus translated our vision of the phenomenon into a model that carries the same assumptions as the BH equation but incorporates spatial changes in A as well as BP-dependent arterial compliance ($\frac{dA}{dP}=C(P)$) (see Figure 2-2). We then derived the

governing nonlinear, partial differential equations of the model and showed that these equations also have a closed-form expression for PWV by generalizing the standard solution. The final equation indeed predicts higher PWV by a BP-dependent amount and, as expected, reduces to the BH equation as changes in A become insignificant with arterial stiffening. Note that relaxing the constant arterial compliance assumption had no impact on the PWV equation. We lastly demonstrated the validity of the proposed equation by showing that it can predict PWV with significantly superior accuracy to the BH equation using a wealth of experimental data from the literature (see Table) including those from early studies (see Figure 2-1A).

To more fully illustrate the difference between the proposed and BH equations, we employ the Langewouters' sigmoidal $A(P)$ model of the human aorta as follows:

$$A(P) = A_{max}\left[\frac{1}{2} + \frac{1}{\pi}\text{atan}\left(\frac{P-P_0}{P_1}\right)\right] \quad \rightarrow \quad C(P) = \frac{dA}{dP} = \frac{A_{max}}{\pi P_1\left[1+\left(\frac{P-P_0}{P_1}\right)^2\right]}, \tag{2.20}$$

where A_{max} is the maximum area at infinite BP; P_0 is the BP at which the arterial compliance is maximal; and P_1 reflects the BP range for which the arterial compliance is relatively constant [30]. Figure 2-3A shows that this model can fit independent and renowned area-BP measurements from *ex vivo* human aortas of different age groups [14]. Substituting Eq. (2-20) into the proposed PWV equation yields a convenient two-parameter equation for relating PWV to BP as follows:

$$v = 0.357\sqrt{\pi P_1\left(1+\left(\frac{P-P_0}{P_1}\right)^2\right)\left(\frac{1}{2}+\frac{1}{\pi}\text{atan}\left(\frac{P-P_0}{P_1}\right)\right)+P}, \tag{2.21}$$

where v is in units of m/s and P is in units of mmHg. Figure 2-3B shows the PWV-BP relationships predicted by Eq. (2-21) with the P_0 and P_1 values obtained via the model fits in Figure 2-3A. For comparison, Figure 2-3B also includes the predictions via the BH equation

(i.e., Eq. (2-21) but with the right-most P set to zero) [31]. This figure shows that the proposed equation makes the most difference when BP is lower and in younger subjects (i.e., where A changes most, as seen in Figure 2-3A). The difference can be dramatic. For instance, a normal PWV of 5 m/s in a 20-24 year old [5] corresponds to a BP at physiologic 80 mmHg for the proposed equation but at non-physiologic 142 mmHg for the BH equation. Note that the lower BP range is crucial and cannot simply be discounted, as PWV is often measured at diastolic BP wherein wave reflection and blood velocity are minimal [2], [5]. Interestingly, unlike the BH equation, the proposed equation also yields a desirable one-to-one relationship between BP and PWV in younger subjects.

Our results also suggest that axial wall tension does not balance the rightward fluid force on the extra arterial cross-sectional area due to the spatial A change and that the actual assumption of the BH equation is that the relative change in A is small compared to the relative change in P [28]. This assumption is not unreasonable, as arteries are much stiffer than veins. However, as the assumption breaks down with decreasing age or BP, the BH equation increasingly overestimates arterial distensibility and becomes a less reliable formula for relating PWV to BP.

Our derivation also results in a modification to the Waterhammer (WH) equation, which may be obtained by combining Eq. (18) with the standard $h(P) = \frac{\rho}{A}$ and $g(P) = C$ and the BH equation (Eq. (2-1)) as follows:

$$v_{WH} = Z^c \frac{A}{\rho} = \frac{dP}{\rho d(\frac{Q}{A})}, \tag{2.22}$$

where $Z^c = \frac{dP}{dQ}$ is the arterial characteristic impedance. This venerable equation indicates that PWV may be measured at a single arterial site (i.e., local, as opposed to regional, PWV) as the slope of BP versus blood velocity (Q/A) during early systole wherein wave reflection is minimal

[32]. However, combining Eq. (2-18) with the proposed $h(P) = \frac{\rho}{A+PC(P)}$ and $g(P) = C(P)$ and the proposed PWV equation (Eq. (2-19)) yields another equation to relate PWV to arterial characteristic impedance as follows:

$$v = Z^c \frac{A(P)+PC(P)}{\rho}. \tag{2.23}$$

This modified equation specifically suggests that the WH equation may similarly underestimate local PWV by a BP-dependent amount.

In conclusion, we have challenged the longstanding BH equation by deriving a PWV equation that incorporates overlooked spatial changes in arterial cross-sectional area and showing that it can significantly improve PWV prediction accuracy. The proposed equation may allow for more precise quantification of arterial stiffening with aging and disease and thus superior cardiovascular risk stratification as well as more reliable calibration of potential PWV-based systems for cuff-less BP measurement.

Chapter 3. Conventional Pulse Transit Times as Markers of Blood Pressure Changes in Human

3.1 Introduction

Current blood pressure (BP) measurement devices employ an inflatable cuff and thus cannot be used anytime or anywhere to manage hypertension. Pulse transit time (PTT) varies inversely with BP in a person due to the physical properties of arteries and can be obtained without a cuff. As a result, PTT is being widely pursued for cuff-less BP measurement [2], [33].

Conventionally, a surrogate of PTT is obtained by using two transducers amongst ECG electrodes and ear, finger, and toe photo-plethysmography (PPG) sensors due to their simplicity and noise robustness and detecting the relative timing between the pair of acquired waveforms [2]. The most popular of these conventional PTTs (cPTTs) has been the time delay between the R-wave of the ECG waveform and the ensuing foot or peak of the finger PPG waveform [2]. This time delay is in fact technically a pulse arrival time (PAT), which includes the pre-ejection period due to the use of the ECG waveform, rather than a true PTT and is referred to as finger PAT here. Similarly, the time delay between a pair of the PPG waveforms is technically a difference between two PTTs and is referred to as dPTT here. For example, the time delay between ear and toe PPG waveforms is called ear-toe dPTT, because it represents the difference between the PTT from the aortic arch to the toe and the PTT from the aortic arch to the ear. Note that the term cPTT therefore denotes a PAT or a dPTT henceforth rather than a true PTT.

Numerous studies have reported that the cPTTs can show inverse correlation with systolic and/or diastolic BP [2], [34]–[41]. However, these studies have often been limited in terms of subjects or BP-varying interventions, so their results may not be generalizable. While studies have examined the PTT-BP relationship under challenging interventions, they have been confined to

animals [39], few healthy humans [40], or critically ill patients [36]–[38], [41] who are often hypotensive and thus not reflective of the hypertension management population. Larger studies of normotensive and hypertensive humans have been conducted, but they have mainly involved few or simple BP interventions [2], [34], [35]. Often times, only exercise has been invoked wherein finger PAT is already known to decline with the parallel increases in systolic and diastolic BP [2]. Furthermore, the previous efforts have typically been limited to study of only finger PAT.

In this study, we compared the cPTTs as markers of BP changes under a battery of nontrivial BP-varying interventions in a relatively large number of normotensive and hypertensive humans.

3.2 Methods

3.2.1 Data Collection

We collected physiologic data from human subjects under a protocol approved by, and in accordance with the relevant guidelines and regulations of, the Institutional Review Boards of University of Rochester and Michigan State University. All subjects gave written, informed consent prior to their participation in the study.

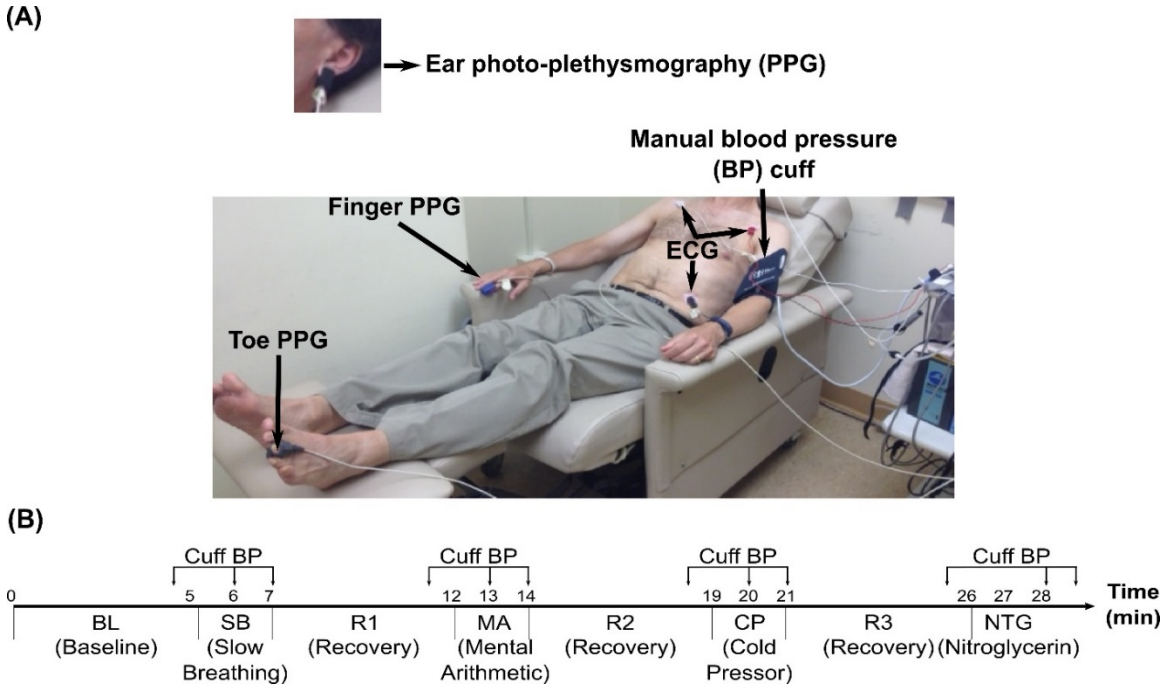

Figure 3-1 Data collection for comparing conventional pulse transit times (cPTTs) as markers of blood pressure (BP) changes in humans.
The **(A)** sensors and **(B)** BP-varying interventions were employed in the reclining volunteer.

We studied the subjects at the University of Rochester's General Clinical Research diThe exclusion criteria included (a) cardiovascular disease exclusive of hypertension that was diagnosed earlier or identified upon physical exam or 12-lead ECG during a screening visit; (b) inter-arm mean BP difference > 10 mmHg during the screening visit; (c) systolic BP < 100 mmHg during this visit; (d) pregnancy; or (e) history of drug abuse or high alcohol consumption rate. A main purpose of the exclusion criteria was to mitigate potential adverse effects of the BP-varying interventions of the study. We enrolled 44 different subjects.

As shown in Figure 3-1A, we placed sensors on each subject as she/he reclined on a chair. The sensors included electrode patches on the chest to measure an ECG waveform (ECG100C, Biopac, USA); transmission-mode PPG clip or soft sensors (8000 series, Nonin Medical, USA) on the earlobe, right fingertip, and toe to measure three PPG waveforms (PPG100C, Biopac); and an

inflatable cuff over the left brachial artery to measure BP (Tycos TR-1, Welch Allyn, USA) via manual auscultation performed by a physician (R. C. B.). We also positioned standard impedance cardiography (ICG) electrodes (NICO100C customized with 4 mA current, Biopac) but found the ICG waveform quality to be poor and aborted this measurement well before study completion. We recorded the waveforms continuously at a sampling rate of 1 kHz using a single data acquisition system (MP150, Biopac). Hence, the waveforms were temporally synchronized.

As shown in Figure 3-1B, we instructed each subject to perform a battery of interventions following a baseline period to change BP. The interventions comprised slow breathing (6 cycles/min for 2-min) to reduce BP[42], mental arithmetic (successively adding digits of a 3-digit number and then adding the sum to the original number for 2-min) to increase BP[43], a cold pressor test (foot immersed in 4° C water for 2-min) to increase BP[44], and sublingual nitroglycerin (0.4 mg tablet under the tongue) to reduce systolic BP but not alter diastolic BP[45]. Five-minute recovery periods occurred between the interventions. For safety considerations, we did not employ nitroglycerin in those subjects with pre-intervention systolic BP < 110 mmHg (19 subjects). As also shown in Figure 3-1B, we made manual cuff measurements of systolic/diastolic BP during baseline, each intervention (at the end and typically the middle), and each recovery period (at the end) for a total of up to twelve sets of four waveforms and BP readings during up to eight different conditions per subject.

3.2.2 **Data Analysis**

As shown in Figure 3-2, we applied strict data exclusion criteria to ensure a meaningful, apples-to-apples comparison of the intra-subject correlations between each cPTT detected from pairs of the waveforms and each BP over the multiple conditions. We visually screened the waveform segments within ±30 sec of each BP measurement for artifact. We selected a >7 sec sub-segment

for which all four waveforms showed minimal artifact. If there was no such sub-segment, we excluded the entire waveform-BP set from further analysis. Our rationale for such exclusion was as follows. In most cases of artifact, not all four waveforms were contaminated. If we kept the measurement set, then the cPTTs detected from the artifact-corrupted waveform(s) would be unfairly handicapped. If we discarded only the noisy waveform(s) in the set, then the cPTTs would not be compared using the same data (e.g., the correlations would be computed based on a different number of data points). If there were two sets of artifact-free waveform sub-segments and BP readings for a condition, we excluded the set with the smaller BP change in order to maximize the intra-subject BP variations. We excluded entire subject records with less than five measurement sets in subjects without nitroglycerin and less than six measurement sets or six measurement sets without three or more interventions in subjects with all four interventions. Our reasoning was that if we kept subjects with few measurement sets, then the computed correlation between cPTT and BP would be misleading (e.g., two data points always yield unity correlation). Hence, a significant fraction of the data were excluded for a valid comparison, but the quality of data from the simple, robust sensors was actually much better.

We analyzed all included waveform sub-segments as follows. We first detected the R-waves of the ECG waveforms using the Pan-Thompkins algorithm. We then detected the peaks of each PPG waveform between successive R-waves. We next detected the feet of the waveforms between the R-waves and successive peaks using the intersecting tangent algorithm[2]. As shown in Figure 3-3, we determined the cPTTs as the time delays (averaged over the sub-segment) between the ECG R-wave and ear PPG foot (ear PAT), ECG R-wave and finger PPG foot (finger PAT), ECG R-wave and toe PPG foot (toe PAT), ear and finger PPG feet (ear-finger dPTT), ear and toe PPG feet (ear-toe dPTT), and finger and toe PPG feet (finger-toe dPTT). For comparison, we also used

the peaks instead of the feet to determine the six cPTTs.

We quantified the strength of the cPTT-BP relationship in each subject using the standard Pearson correlation coefficient. Another metric that has been previously employed for quantifying the PTT-BP relationship strength may be obtained by fitting a curve (e.g., BP = m·cPTT+b) through the cPTT and BP pairs of a subject and then computing the standard deviation (SD) of the fitting error in units of mmHg [2], [33]. However, the correlation coefficient is preferred to this BP error SD for two reasons. One reason is that the correlation coefficient takes the sign of the relationship into account. That is, cPTT and BP should be negatively correlated. So, if cPTT and BP showed positive correlation in a subject, the correlation coefficient would penalize for this non-physiologic relationship through its sign. In contrast, the BP error SD is blind to the sign of the correlation. For example, if cPTT and BP showed strong, positive correlation in a subject, then the BP error SD would be small despite the non-physiologic relationship. The second reason is that the correlation coefficient takes the size of the BP variations within a subject into account. That is, the square of the correlation coefficient (a.k.a., R^2) indicates the fraction of the total BP variance that is explained by a cPTT. In contrast, the BP error SD strongly depends on the intra-subject BP variation size. For example, if the intra-subject BP changes were small, then the BP error SD would be low even with no cPTT-BP correlation. (In such a case, the BP error SD would simply equal the BP SD.) For these reasons, the BP error SD was misleading here, so we only employed the correlation coefficient.

We arrived at one correlation coefficient for each cPTT and each BP per subject. We compared the mean correlation coefficients (i.e., the average of the correlation coefficients over the subjects) of the six cPTTs for each BP. Since there were more than two mean correlation coefficients, we conducted this comparison using one-way repeated measures ANOVA. When this test yielded p

< 0.05, we performed pairwise comparisons using a Tukey test, which corrects for the multiple comparisons. We also performed paired t-tests when comparing two mean correlation coefficients.

3.3 Results

As shown in Figure 3-2, a total of 214 sets of cPTTs and manual cuff systolic/diastolic BP readings from 32 subjects (50% female; 52 (17) (mean (SD)) years of age; 166 (10) cm in height; 89 (34) kg in weight; 31% with smoking history; 9% with LDL cholesterol >=190 mg/dL) were included. Eight subjects self-reported as hypertensive and were taking medications (e.g., Hydrochlorothiazide, Atorvastatin, Metoprolol, Lisinopril, Losartan, Aspirin, and Amlodipine).

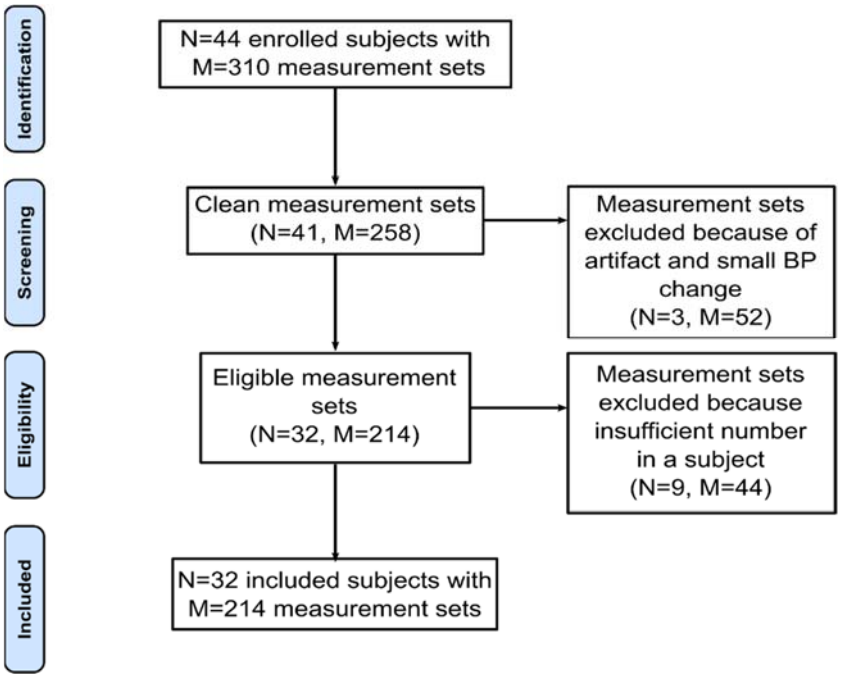

Figure 3-2 Data exclusion criteria with number of included and excluded subjects and measurement sets. A measurement set comprises the ECG waveform, ear, finger, and toe photo-plethysmography (PPG) waveforms, and manual cuff BP for a subject and condition (see Figure 3-1B). The criteria were strict to ensure a valid comparison of cPTTs as markers of BP changes.

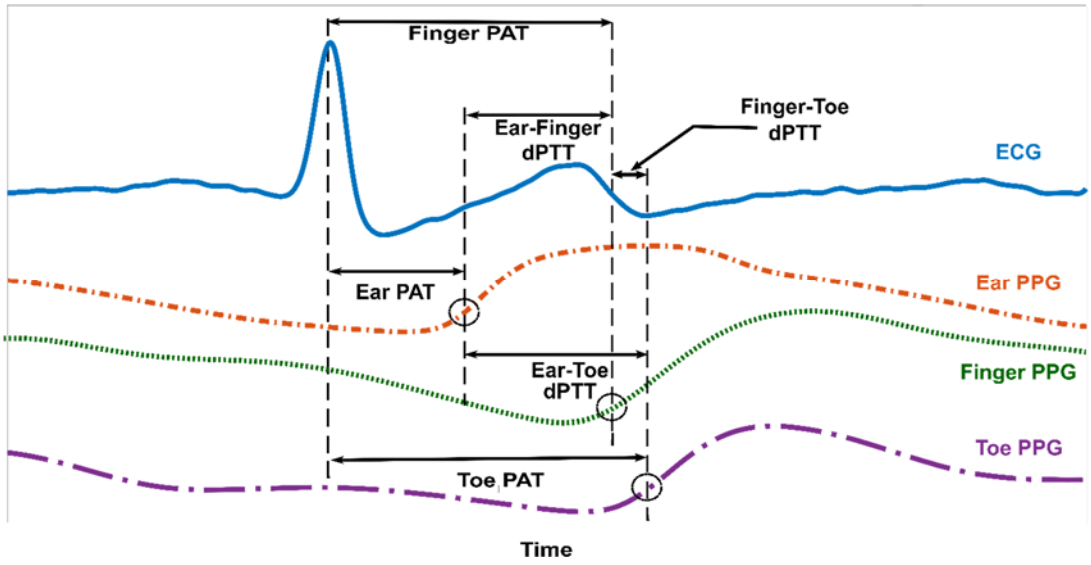

Figure 3-3 Data analysis for comparing cPTTs as markers of BP changes in humans.
The six detected time delays include three pulse arrival times (PATs) and three differences between two PTTs (dPTTs). The time delays were averaged over multiple beats and compared in terms of tracking the intervention-induced BP changes via the intra-subject correlation coefficient.

Figure 3-4 shows the mean (with SE) over the subjects of each cPTT shown in Figure 3-3 and each BP for the baseline period, four interventions, and three recovery periods. (Note that we did not normalize each cPTT for wave travel distance per subject, as the height of the subjects varied little.) The baseline (BL) systolic and diastolic BP were 121±3 and 79±2 mmHg (where X±Y denotes mean of X and SE of Y over the subjects here and henceforth). The subject cohort thus constituted mainly normotensives and controlled hypertensives. The baseline (BL) ear, finger, and toe PATs were 126±4, 269±6, and 266±5 msec, respectively. While these values are consistent with previous data[2], the comparable magnitudes of the finger and toe PATs may be in part due to a hydrostatic effect in the reclining subject (see Figure 3-1A). In particular, the effective BP for finger PAT may be lower than that for toe PAT so as to increase finger PAT relative to toe PAT. Hence, BL ear-finger dPTT (which also equals finger PAT – ear PAT) and ear-toe dPTT (which also equals toe PAT – ear PAT) were comparable in magnitude, whereas BL finger-toe dPTT

(which also equals toe PAT – finger PAT) was near 0 msec. Slow breathing (SB) caused little change in BP on average (see Figure 3-4). As expected and on average, mental arithmetic (MA) and cold pressor (CP) increased systolic and diastolic BP, whereas nitroglycerin (NTG) reduced systolic BP but did not alter diastolic BP (see Figure 3-4). Overall, the interventions caused systolic and diastolic BP to range respectively over 25±1 and 15±1 mmHg per subject (result not indicated in Figure 3-4). Further, the correlation coefficient between systolic and diastolic BP was 0.49±0.07. Hence, the two BP levels did not merely change in parallel. The range of the cPTTs were similar with an overall mean of 26±3 msec per subject (result not indicated in Figure 3-4). As can be seen in Figure 3-4, the toe PAT trend showed the best inverse correlation with the systolic BP trend, while the toe PAT and finger PAT trends showed the best inverse correlation with the diastolic BP trend. The other cPTT trends did not appear to correlate well with either of the two BP trends.

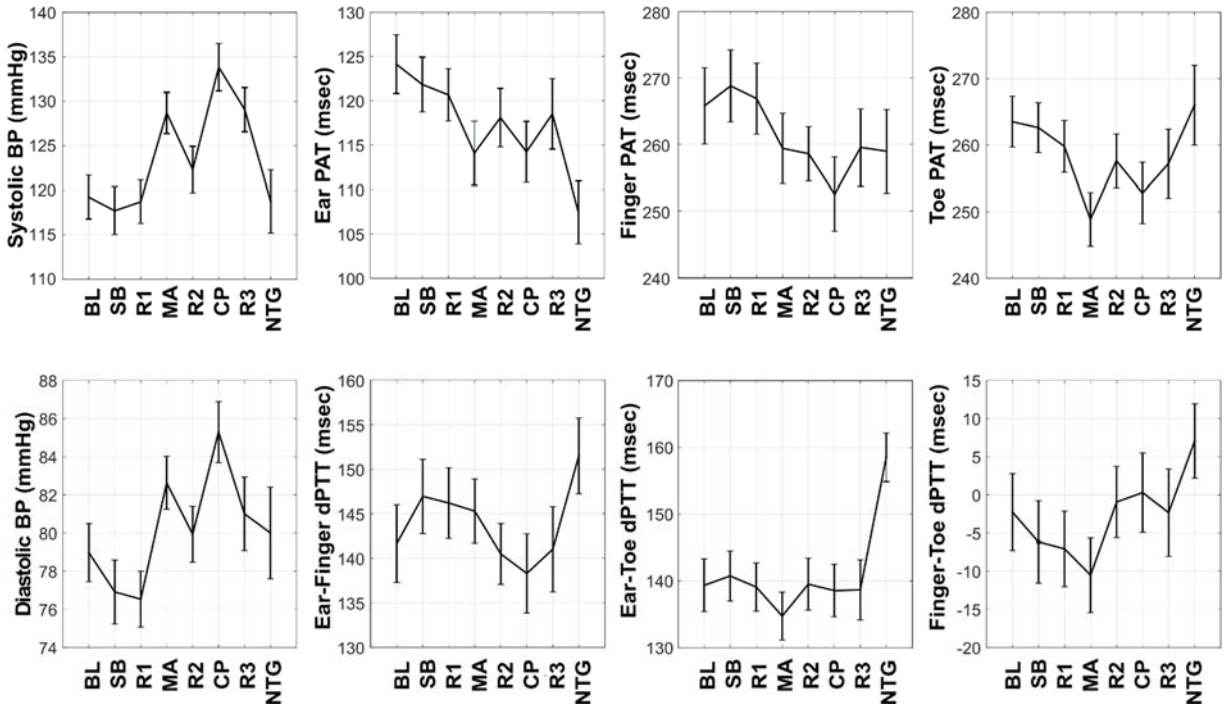

Figure 3-4 Mean (with SE) over the subjects (N = 32) of systolic and diastolic BP and the cPTTs for the baseline period, each intervention, and each recovery period (see Figures 3-1 and 3-3 for definitions of interventions and cPTTs).

The toe PAT trend appeared most inversely related to the systolic BP trend, whereas the toe PAT and finger PAT trends appeared most inversely related to the diastolic BP trend.

Figure 3-5 shows the mean (with SE) of the correlation coefficients between each cPTT shown in Figure 3-2 and each BP over the subjects as well as the results of one-way repeated measures ANOVA and the Tukey test. These correlation coefficients significantly differed for the two BP levels. Toe PAT tracked both BP levels best. The correlation coefficients were appreciably higher for systolic BP than diastolic BP. The correlation coefficient between toe PAT and systolic BP was -0.63±0.05, the only one above 0.5 in magnitude, and 54% higher in magnitude than the corresponding correlation coefficient for the popular finger PAT.

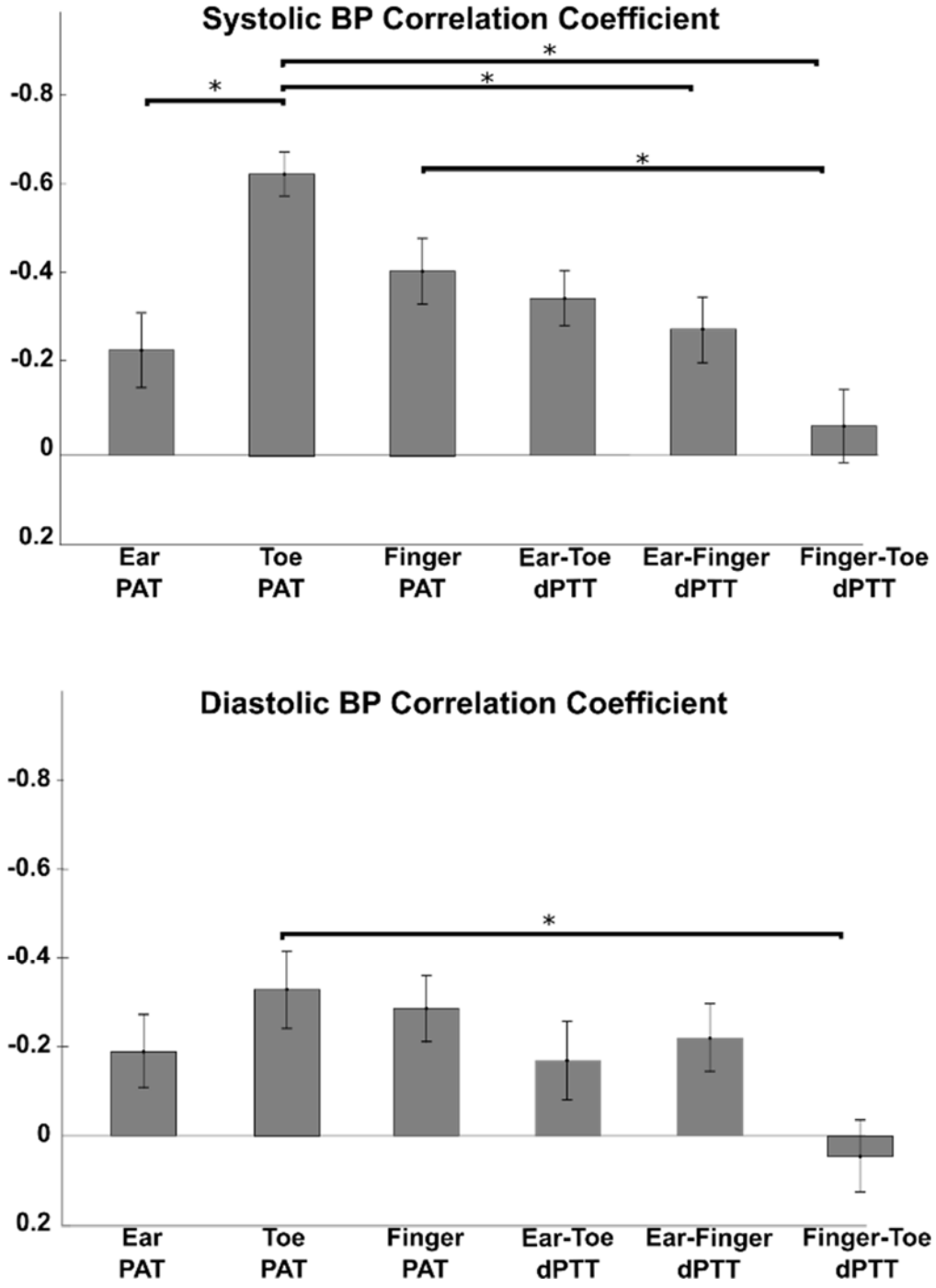

Figure 3-5 Mean (with SE) of the correlation coefficients between each cPTT and each BP over the subjects (see Figures 3-1 and 3-3 for cPTT definitions).

The correlation coefficients differed significantly for both systolic and diastolic BP according to one-way ANOVA. *indicates significant pairwise differences based on a Tukey test. The best correlation by a substantial extent was between toe PAT and systolic BP.

The mean correlation coefficients between each cPTT detected via the PPG waveform peaks (instead of feet) and each BP over the subjects were all substantially lower than those shown in Figure 3-5. Figures 3-6 shows an examplary comparison of the mean (with SE) of the correlation coefficients of toe PAT detected via the PPG waveform foot and peak and systolic BP over the subjects ($p \leq 0.001$ as per a paired t-test).

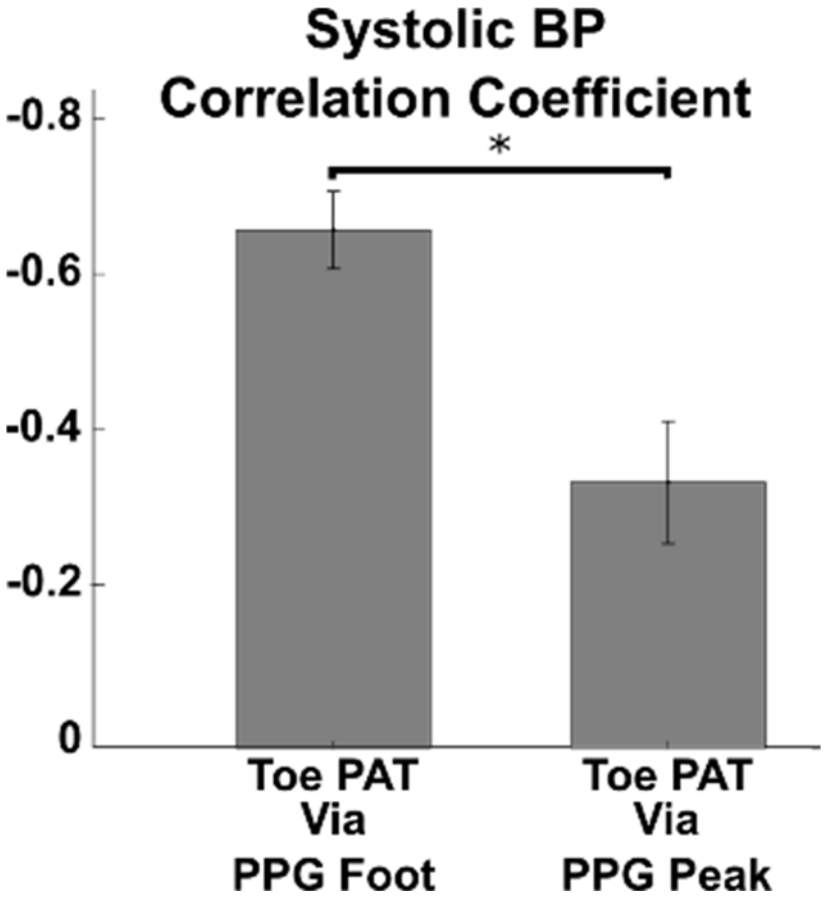

Figure 3-6 Mean (with SE) of the correlation coefficients between toe PAT detected via the PPG foot (see Figure 3-3) and peak and systolic BP over the subjects.

*indicates significant difference based on a paired t-test. Toe PAT detected via the PPG foot afforded much better correlation.

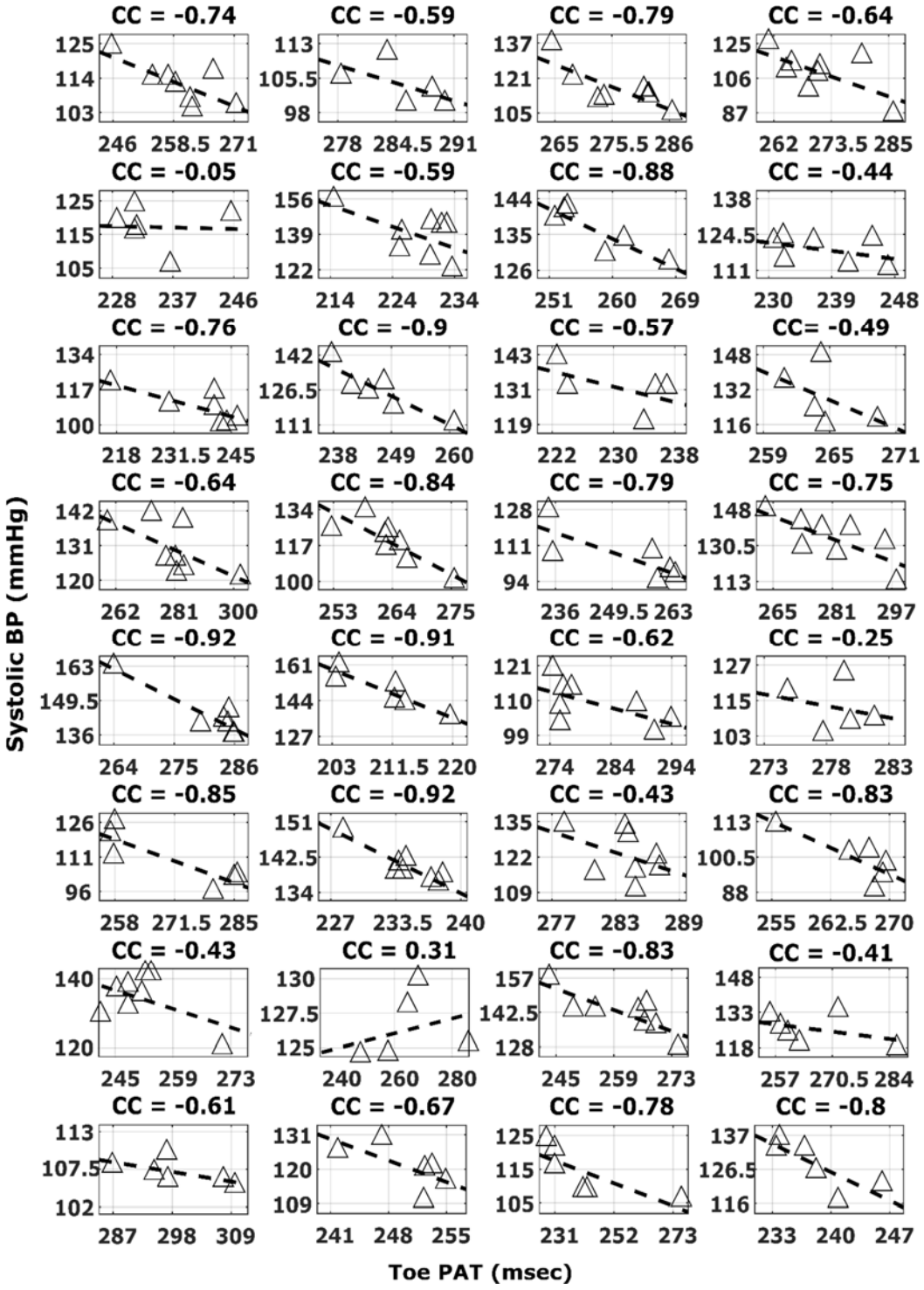

Figure 3-7. Subject-by-subject plots of systolic BP versus toe PAT detected via the PPG foot (see Figure 3-3).

Red lines are lines of best fit. The correlation coefficient (CC) varied per subject.

In sum, the best correlation by a substantial extent was between toe PAT detected via the PPG

waveform foot and systolic BP (-0.63±0.05 correlation coefficient). Figure 3-7 shows subject-by-subject plots of this toe PAT versus systolic BP for all 32 subjects.

3.4 Discussion

In this study, we compared cPTTs detected from ECG, ear, finger, and toe PPG waveforms in terms of tracking BP changes induced by interventions in humans. Our study may be notable relative to previous efforts in that it comprised (1) a relatively large number of human subjects (N = 32; see reference[2] for N of similar studies) with appreciable diversity (25% hypertensive and average age of 52±17 years); (2) acquisition of multiple cPTTs instead of just the popular finger PAT (see Figures 3-1A and 3-3); (3) manual cuff BP measured by a physician rather than typically used but less accurate automatic cuff BP readings; and (4) a battery of interventions to change BP nontrivially instead of just typical exercise (see Figurs 3-1B and 3-4).

The most important of these strengths may be the interventions, which comprised slow breathing, mental arithmetic, a cold pressor test, and sublingual nitroglycerin. Although a previous study showed that two minutes of slow breathing reduces BP, especially in hypertensives[42], this intervention had minimal impact on BP here (see Figure 3-4). However, mental arithmetic increased systolic and diastolic BP via mainly an inotropic effect[43]; cold pressor increased systolic and diastolic BP via mainly vasoconstriction [44]; and nitroglycerin reduced systolic BP without changing diastolic BP via a vasodilatory effect [45] (see Figure 3-4). As a result, these interventions collectively caused systolic and diastolic BP to change appreciably (25±1 and 15±1 mmHg) and not merely in parallel (intra-subject correlation coefficient of 0.49±0.07). In this way, we could not only determine the cPTT with the best association with BP but even determine the relative association with systolic and diastolic BP. Interestingly, the PPG amplitude increased with mental arithmetic and sublingual nitroglycerin and decreased with cold pressor (result not

shown), suggesting that PPG amplitude may not readily indicate BP changes. The likely reason is that the amplitude of the PPG, which indicates blood volume, is approximately equal to the product of local arterial compliance and pulse pressure and that compliance changes with smooth muscle contraction (e.g., compliance decreases during cold pressor such that the PPG amplitude decreases despite the increase in pulse pressure shown in Figure 3-4).

We found that toe PAT (the time delay between the ECG R-wave and the ensuing foot of the toe PPG waveform) was best in tracking the intervention-induced BP changes amongst six cPTTs (see Figure 3-5). The next best cPTT as a marker of BP changes was the popular finger PAT (the analogous time delay via the finger PPG waveform). However, toe PAT afforded 54% better correlation with systolic BP than finger PAT (see Figure 3-5).

Despite being detected at the level of diastole of the PPG waveform, toe PAT (and the other cPTTs) correlated much better with systolic BP than diastolic BP (see Figure 3-5). One reason may be that toe PAT includes the pre-ejection period (PEP), which, like systolic BP, is partly determined by ventricular properties[2]. Another reason is that nitroglycerin decreased systolic BP, did not alter diastolic BP, and increased toe PAT via smooth muscle relaxation. Hence, toe PAT changed opposite to systolic BP, but not diastolic BP, during nitroglycerin (see Figure 3-4). However, this result may be serendipitous, as the toe PAT increase during nitroglycerin may have been due to smooth muscle relaxation rather than the systolic BP decline. On the other hand, the correlations between each cPTT and BP were similar in the subjects who received nitroglycerin versus the subjects who did not receive the intervention (results not shown).

Detecting toe PAT (and the other cPTTs) using the PPG waveform peaks yielded substantially lower correlations with BP (see Figure 3-6). This finding is not surprising, because the time delay between the foot and ensuing peak of the PPG waveform is largely determined by ventricular

properties. In a recent study, we showed that PPG sensor contact pressure, which was controlled in the present study, impacts finger PAT detected via the PPG waveform peak twice as much as finger PAT detected via the PPG waveform foot [46]. Taken together, the pair of studies indicate that PTT should be detected specifically via the feet of PPG waveforms.

Hence, the best correlation by a substantial extent was between toe PAT detected via the PPG waveform foot and systolic BP. However, the correlation coefficient was only -0.63±0.05.

These findings (see Figure 3-4 and 3-5 in particular) may be the result of numerous, complicating factors, so a unifying interpretation may be impossible. Generally speaking, major factors limiting the correlation are that the PATs include PEP, which is again determined by ventricular properties rather than just BP, and that all cPTTs excluding toe PAT include substantial wave travel time through smaller, muscular arteries wherein smooth muscle contraction/relaxation can cause the time delay to vary independently of BP [45]. Another factor limiting the correlation for the dPTTs could be that detection of the PPG waveform feet is less robust than detection of the ECG waveform R-wave.

In contrast to many previous studies of finger PAT during exercise, our results indicate that finger PAT does not provide good correlation with systolic or diastolic BP. So, even though convenient devices can be developed to obtain finger PAT (e.g., smartwatch form factor), such efforts may not be worthwhile for cuff-less BP tracking. Our results indicate that it may make more sense to build devices to measure toe PAT. Note that building a convenient, portable system to measure toe PAT would be more challenging than finger PAT (as two recording devices may be needed). However, our study, instead, suggests that it may be necessary to obtain innovative PTTs to improve the correlation with BP via novel sensors and/or waveform detections. Innovative sensors may include ballistocardiography [47], seismocardiography [48], [49], wrist

bioimpedance [50], ultrasound [51], and radar sensors [52]. Unlike ECG and PPG waveforms, these sensors may afford true PTT rather than dPTT or PAT. However, they may be more complicated and/or less robust to artifact. Innovative waveform detections may include system identification methods to more robustly extract the PTTs from the entire waveforms rather than just their feet [53] or to extract true PTT rather than dPTT from two distal waveforms [54]. However, advanced methods beyond waveform feet detection require much more proof.

Our study does have limitations. Firstly, while the number of subjects is relatively large compared to similar studies, this number is small compared to standardized protocols, and a quarter of the subjects were excluded for a meaningful, apples-to-apples comparison. Secondly, the interventions did change systolic and diastolic BP appreciably but not as much as we hoped. Thirdly, although 25% of the study cohort were self-reported hypertensives, these subjects had their BP under control on average. Fourthly, the impact of medications on the results was not assessed. Future studies of cPTTs should include more subjects, uncontrolled hypertensives, the same subjects with and without medications, and, if possible, interventions that produce more extensive BP changes. We do anticipate that such studies may reveal further limitations of cPTTs as markers of BP changes.

In conclusion, finger PAT and cPTTs detected via the PPG waveform peaks may not generally correlate well with BP in a person. Toe PAT may be a superior marker of changes in systolic BP in particular but perhaps not good enough. Innovations are needed in order to achieve cuff-less BP measurement via PTT.

Chapter 4. Assessment of the Calibration Model for Computing Blood Pressure from Pulse Arrival Time or Photoplethysmography Features after One Year of Aging

4.1 Introduction

Pulse transit time (PTT) is a potential, physics-based approach for achieving passive, cuff-less blood pressure (BP) monitoring. PTT is detected via the time delay between proximal and distal arterial waveforms and then mapped to BP using a calibration model constructed from previous PTT-cuff BP measurement pairs. In addition to PTT, PPG waveform analysis is another popular approach for cuff-less blood pressure monitoring. PPG waveform features like Slope Transit Time (STT- PPG amplitude divided by maximum derivative) which is unitless, must be calibrated to BP in the unit of mmHg to construct a calibration model.

While it is known that the calibration model must be updated periodically to account for aging effects, data on the time period required for these "cuff re-calibrations" are scant. Some studies are too short and some study are just for finger and not other body location measurement [55].

The objective of this study was to determine how much calibration Models change after one year and how effective the calibration model is in measuring BP one year later. We previously collected data and developed calibration models relating PTT or PPG waveform features to BP using cuff BP and battery of intervention in various locations and repeated a study two times one year apart. Our main experimental finding showed that the Toe PAT-BP calibration model is effective after one year. This model did not change significantly such that it could predict systolic blood pressure reasonably well a year. This knowledge could help in the development of BP monitoring system.

4.2 Material and Methods

The objective of this We explained our human data collection in detail elsewhere [56]. Briefly, the study was approved by our Institutional Review Boards, and we obtained written, informed

consent from the subjects. We studied seven volunteers (54±8 years, 5 male, 1.68±0.02 m) in three recording sessions that occurred one year apart. In each session, our recordings included the ECG waveform, toe photo-plethysmography (PPG) waveform, ear PPG, finger PPG, and auscultation cuff BP before and after mental arithmetic, a cold pressor test, slow breathing, and sublingual nitroglycerin as shown in Figure 4-1.

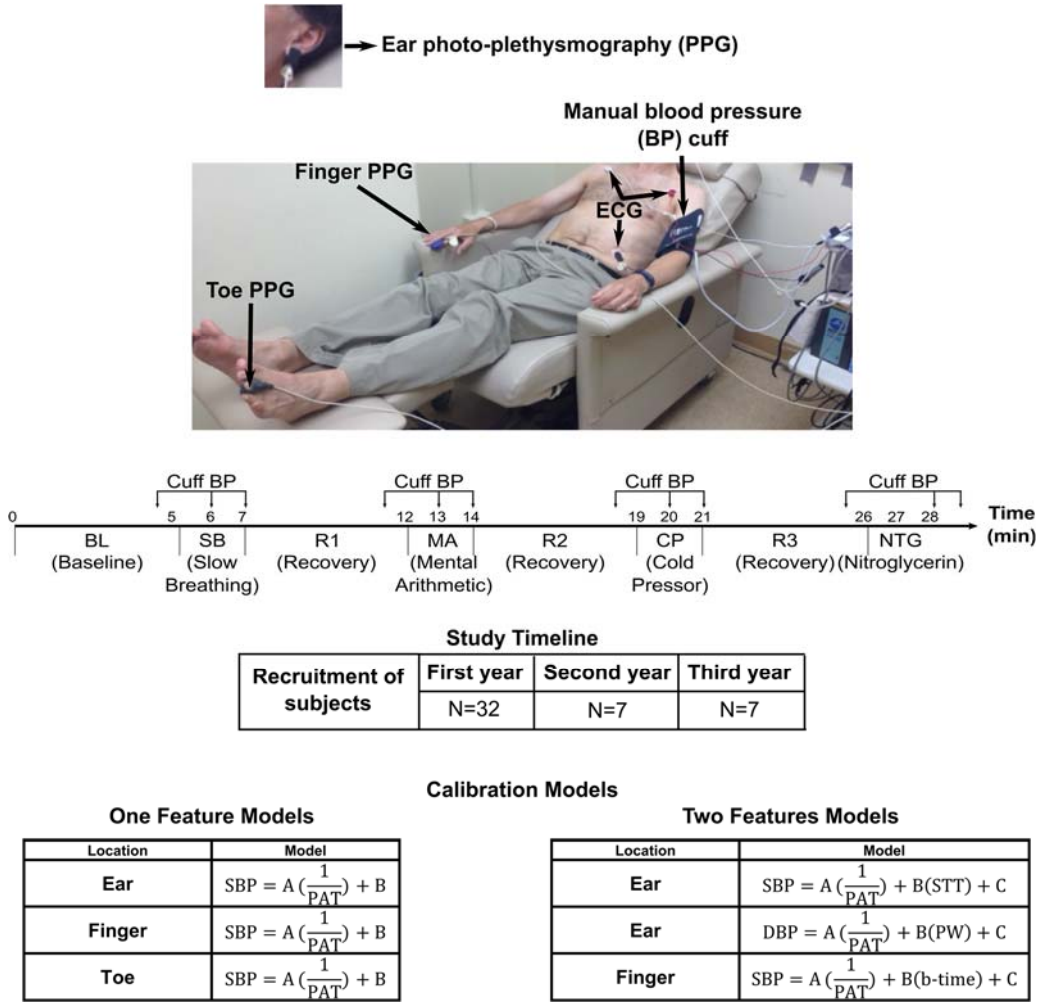

Figure 4-1 The overall approach of study.

By collecting data on a large cohort of subjects with the battery of intervention in three sessions over two years, we created six calibration models in which PTTs or PPG waveform features related to BP.

We intended to study after one and two years, but due to the acclimatization issue, the first session thus allowed the subjects to acclimate to the protocol. Based on the first session, we developed six calibration models related PTTs or PPG waveform features to blood pressure on large cohort of the subjects. Three models had one feature, and the other had two features. We then fitted a line

between feature-BP data pairs or a plane between features-BP data pairs for each subject to form a person-specific calibration model for the second session (baseline) and the third session (one year later). We calculated the difference between group average calibration curves for the baseline period and one year later to mitigate randomness (getting rid of scattering) and isolate the impact of aging. By using root-mean-squared-error (RMSE), we quantified the overall difference after one year.

Next, we examined our six calibration models by determining coefficient based on the second session and testing performance on the third session (after one year). We also developed two reference models as the worst-case and the best-case. In the worst-case, we used the average of all cuff-BP measurements of the second session to predict the third session (using no model). In the best case, we trained and tested our model just on the third session to get the lower bound of the best possible result (due to overfitting noise).

We used RMSE metric to perform statistical comparison. In each subject for all models, we computed RMSE and then took the average over all the subject. We did t-test to statistically compare between models.

4.3 Results

Figure 4-2 shows the difference between the group average calibration models for the baseline period and one year later. It was a line for one feature calibration model, while for calibration models with two features, it was a plane. Among all, the bias and precision error of the Toe systolic model and finger systolic model in one feature calibration model and finger systolic model in two features calibration model are in an acceptable limit.

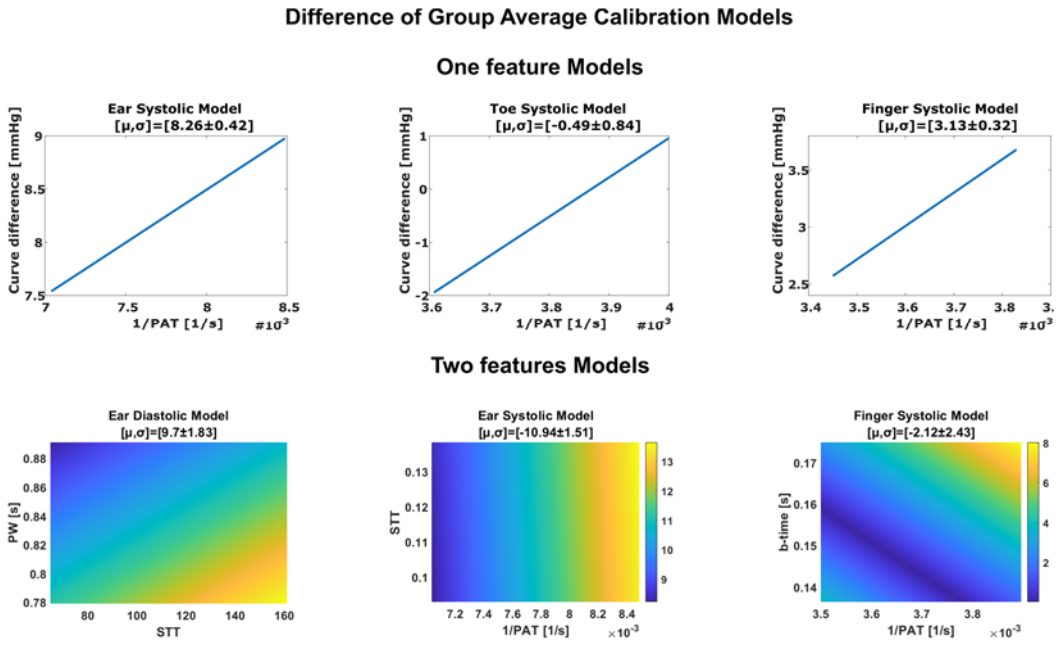

Figure 4-2 Difference between the group average calibration models for the baseline period against one year later.

Figure 4-3 shows the result of the prediction of the third session versus measurement. This table also represents the statistical comparison between calibration models and the best and worst-case scenarios. When there is no statistical significance between the calibration model and the worst case in which employs the average of cuff measurement, the calibration model did not offer any value. Furthermore, this table includes results before and after applying robust method for detecting outliers. We considered any element greater than three scaled Medina Absolute Deviation (MAD) from median as a outlier.

Body Measurement Location		RMSE between measurement and prediction for			P value	
		The best	Model (using features)	The worst (no features used)	The best versus models	The worst versus model
One feature Models						
Toe	Before removing outliers	6.80±1.19	12.11±1.95	14.52±1.62	0.001*	0.03*
	After removing outliers	6.21±0.86	9.70±0.82	13.19±1.12	0.003*	0.04*
Finger	Before removing outliers	7.93±1.29	13.74±2.25	14.52±1.62	0.06*	0.8
	After removing outliers	7.29±1.02	10.68±1.06	13.19±1.12	0.03*	0.14
Ear	Before removing outliers	7.82±1.05	13.79±1.90	14.52±1.62	0.001*	0.56
	After removing outliers	7.29±0.82	11.60±1.58	13.19±1.12	0.01*	0.33
Two features Models						
Finger	Before removing outliers	5.75±1.01	13.42±2.61	14.52±1.62	0.03*	0.76
	After removing outliers	4.57±0.45	11.92±1.50	13.19±1.12	0.004*	0.54
Ear (Systolic)	Before removing outliers	6.55±1.28	13.32±2.01	14.52±1.62	0.001*	0.39
	After removing outliers	4.10±0.57	12.16±1.19	13.19±1.12	0.0001*	0.48
Ear (Diastolic)	Before removing outliers	3.77±0.68	8.41±1.72	5.72±1.19	0.01*	0.06
	After removing outliers	3.07±0.36	7.24±0.99	4.63±0.43	0.008*	0.01*

* - Statistically Significant

Figure 4-3 Difference between the group average calibration models for the baseline period against one year later.

Median Absolute Deviation (MAD) method employed as robust method for detecting outliers. P-value less than 0.05 considered as a statistical significant.

Figure 4-4 shows correlation and Bland-Altman plots of systolic BP estimated by invoking the baseline calibration curve (second session) to one year-later (third session) toe PAT measurement versus reference cuff systolic BP. Excluding the three outliers, the bias and precision errors were -1.3 and 9.7 mmHg, near the well-known acceptable regulatory limits of 5 and 8 mmHg.

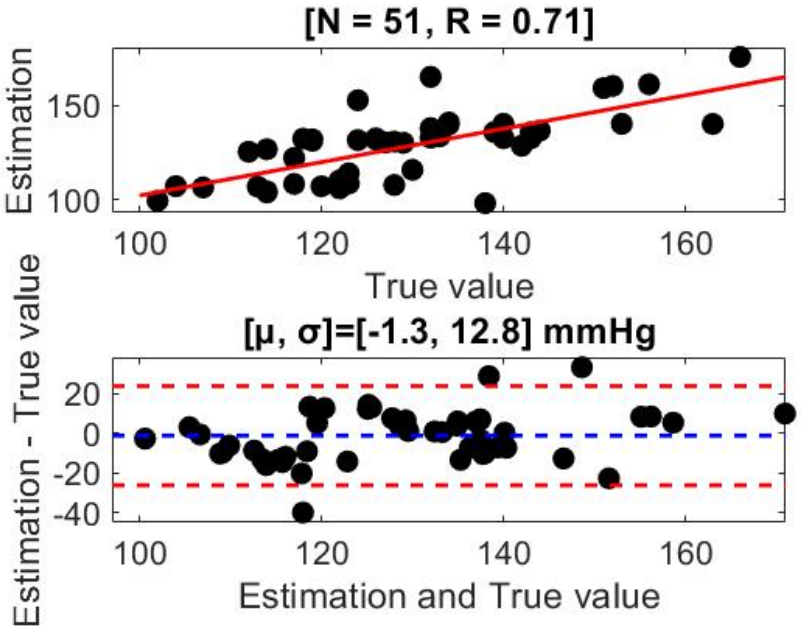

Figure 4-4 Correlation and Bland-Altman plots of one-year-later systolic BP estimated with the baseline calibration curve versus reference systolic BP

4.4 Discussion

PTT and PPG waveform analysis are popular approaches for cuff-less BP monitoring. Numerous studies reported calibration models relating PTTs or PPG waveform features to BP. While it is known that the calibration curve must be updated periodically to account for aging effects, data on the time period required for these "cuff re-calibrations" are scant, and it is not clear how long the calibration curve of these models holds up!

We first developed six calibration models relating PTTs, and PPG waveform features to BP for achieving this goal. Then we repeated the experiment on seven people for two years to see how much calibration models change after one year. Based on our experimental evidence, we found that the Toe PAT calibration model works well and could be calibrated after one year. These results are consistent with a previous theoretical study in which we predicted that annual cuff re-

calibrations would be necessary for 50 year olds [57]. By removing outliers based on the MAD robust method, the error of prediction of visit three based on visit 2 is eight mmHg. Toe PAT is mainly aorta and is not affected by the smooth muscle.

The Finger PAT calibration model had value, but it's not as well as the Toe PAT calibration model. Smooth muscle contraction (SMC) could be a factor [2]. This model may require a shorter calibration period.

All other four calibration models were not good, and they were not helpful after one year. Firstly, SMC could be one factor. Secondly, B-time and STT (feature used in calibration models) were not robust because they related to viscoelasticity and SMC impacts it. Thirdly, there is a lot of compensatory mechanism in the head that affects all the ear calibration models.

Using all interventions is crucial to train the calibration models. Using just MA, or CP, or SB intervention for determining the Toe PAT calibration model coefficient, we got 50 mmHg, 40 mmHg, 22 mmHg RMSE err, which is very bad.

Our experimental findings suggest that cuff re-calibrations of PTT-based BP measurement systems may occur every year, which is quite practical. These results are consistent with a previous theoretical study in which we predicted that annual cuff re-calibrations would be necessary for 50 year olds.

Our study does have some limitations. The main limitation of the study is the small number of subjects, mainly because of the pandemic. The covid-19 pandemic stopped our subject recruitment. Another reason was the battery of challenging interventions that did not allow collecting data easily from many subjects quickly. We still found statistical significance in the Toe calibration model with these seven subjects, which showed our data is enough in this case. Another limitation

is that we couldn't study the impact of age. To investigate the effect of age, we need to collect data from subjects of the same age which pandemic and challenging intervention stopped this goal.

This study concludes a series of studies on PTT/PPG for cuffless BP. In the first study, we showed that toe PAT is by far best compared to conventional PTTs [56]. In second study, we showed adding PPG features can help ear and finger locations, but toe PAT still was a bit better on average [58]. In this study, we showed that toe PAT model is valid longer than other models and at least for a year. Taken together, this trio of studies supports toe PAT for cuffless BP. The challenges are to create a convenient recording device and a practical way to accurately determine the model coefficients. Further studies of toe PAT as a marker of BP in more subjects are also needed to confirm our findings.

Chapter 5. Towards a Convenient, Non-Imaging Device for Abdominal Aortic Aneurysm Screening and Surveillance

5.1 Introduction

An aortic aneurysm is a balloon-like bulge in the main artery supplying blood to the body. In this condition, a weakened aortic wall in concert with the distending BP causes progressive vessel expansion and, in some cases, rupture. A ruptured aorta has a mortality rate of ~80% [59], [60].

Aneurysms are more common in the abdominal aorta than in the other part of the aorta [61]. An abdominal aortic aneurysm (AAA) is often defined as a vessel segment > 3.0 cm in diameter [59], [60]. AAA is a top 15 leading cause of death in the US [60]. While the prevalence of AAA may have recently declined, likely due to a reduction in smoking [62], the future occurrence of AAA could increase substantially as society ages [63].

AAAs can be accurately diagnosed with an expert's imaging methods, including ultrasound, CT, and MRI. Ultrasound is preferred because it has high sensitivity (94-100%) and specificity (98-100%) and is safe and lower in cost [59], [60]. Aortic aneurysms can be treated via surgery, either open or endovascular repair. The mortality rate of surgical repair can be just 2-3% [60], [64]. Since most aortic aneurysms are asymptomatic, screening and surveillance are essential [59], [60], [64].

However, these methods require an expert operator. They are expensive, and AAA is considerably under-detected at present [59] and may become even more under-detected in the future as the disease prevalence increases with societal aging. Our broad goal is to establish a convenient device in use and cost for AAA screening and surveillance.

In this study, we hypothesized that arterial waveforms due to increasing diameter (Figure 5-1A) or early wave reflection (Figure 5-1B), which could be obtained with such a device, constitute a

non-imaging solution for indicating aneurysm size. We tested this physiologically based hypothesis efficiently and effectively via analysis of a wealth of existing patient data. Our finding suggested that features of carotid and femoral artery waveforms could be used as markers of abdominal aortic aneurysms (AAA) in patients. This knowledge may ultimately translate to a convenient device that helps reduce aortic aneurysm mortality.

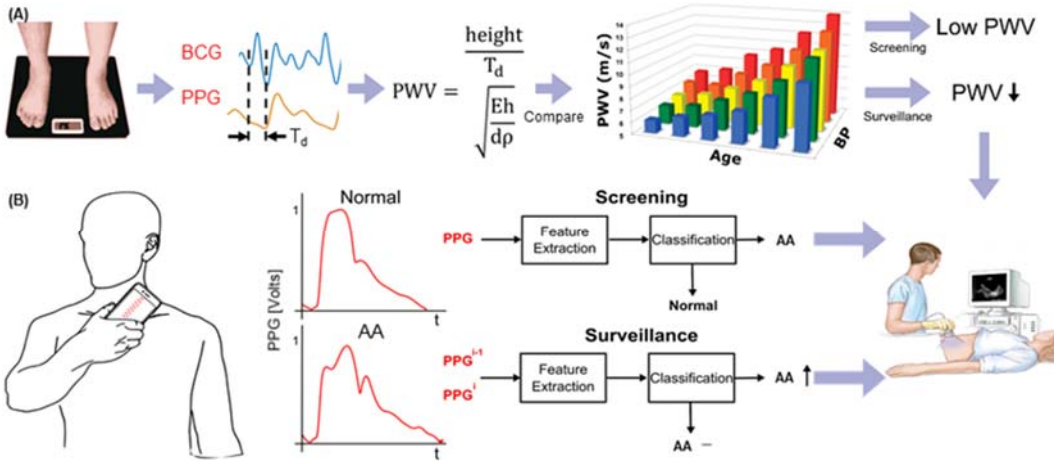

Figure 5-1 Potential convenient, point-of-care devices for aortic aneurysm (AA) screening and surveillance.

The hypothesis underlying the (A) weighing scale- and (B) smartphone-based devices is that arterial waveforms (e.g., ballistocardiography (BCG) and photo-plethysmography (PPG) waveforms) indicate AA size. For example, pulse wave velocity (PWV) via the time delay (Td) between two waveforms decreases with increasing AA diameter (d), while waveform undulations appear due to negative wave reflection induced by the AA. These devices may be best used to indicate if an accurate, but less convenient, ultrasound scan should be ordered or not.

5.2 Material and Methods

In this paper, we analyzed the existing AAA patient database. We extracted physiology-inspired waveform features and determined regression coefficients using stepwise regression with the reference abdominal aortic diameter as the dependent variable. We also applied leave-one-out cross-validation to compare the predicted and reference abdominal aortic diameters.

5.2.1 **Human Physiologic Data**

This database was described in detail previously [65]. Briefly, the database included carotid and femoral artery tonometry waveforms, the physical distance between the carotid and femoral arteries (D), and arm cuff blood pressure (BP) values, and reference abdominal aortic diameter via imaging from 50 anonymized AAA patients before and three weeks after endovascular repair (EVAR). In 17 of these patients, the exact measurements were also available three years after EVAR. Furthermore, this database included 50 control subjects matched in various ways, including age and BP. The patients were old (66±10 years) and predominantly male (90%), and many had comorbidities (e.g., hypertension) and were on medications (e.g., beta-blockers). Table 5-1 shows detailed individual information and statistical comparison for AAA patients against matched control.

Table 5-1 Individual characteristics comparison between AAA patient and matched control.

	AAA	**Control**	**P value**
N	50 (v1 and v2)	50	-
Age (year)	66	61	0.07
Female (n)	5	5	1
SBP,MBP,DBP [mmHg]	132,99,78	137,102,80	0.13,0.29,0.26
Height [cm]	168	163	0.001
Weight(Kg)	68	64	0.06
Smoking (n)	27	10	0.003
Diabetes	8	6	0.56
HR (bpm)	67	74	0.002

5.2.2 Data Analysis

We analyzed this data to determine if the carotid-femoral waveform feature could improve the prediction of AAA diameter.

5.2.2.1 Pre-Processing

For removing noise and keeping the carotid-femoral waveform details, we used a bandpass filter with cutoff frequencies of 0.5 to 10 Hz. Then by finding five shape-wise similar beats in each segment and taking an average over these five beats, we ended up with an ensemble-averaged representative beat.

5.2.2.2 Feature Extraction

We considered two sets of features, namely baseline features and arterial waveform features. In baseline features, we used demographic information such as age, height, weight, body surface area (BSA), and individual clinical information such as systolic blood pressure, diastolic blood pressure, smoking history, and diabetes. In arterial waveform features, we extracted three physiologically inspired features.

One feature was the ratio of carotid-femoral pulse wave velocity (PWV) to diastolic BP and age. PWV decreases with increasing aneurysm diameter per the Moens-Korteweg equation and decreases with decreasing age and BP due to the nonlinear properties of the arterial wall. As shown in Figure 5-2, PWV (=D/PTT) was detected at the level of diastolic BP via the foot-to-foot time delay between the carotid and femoral waveforms.

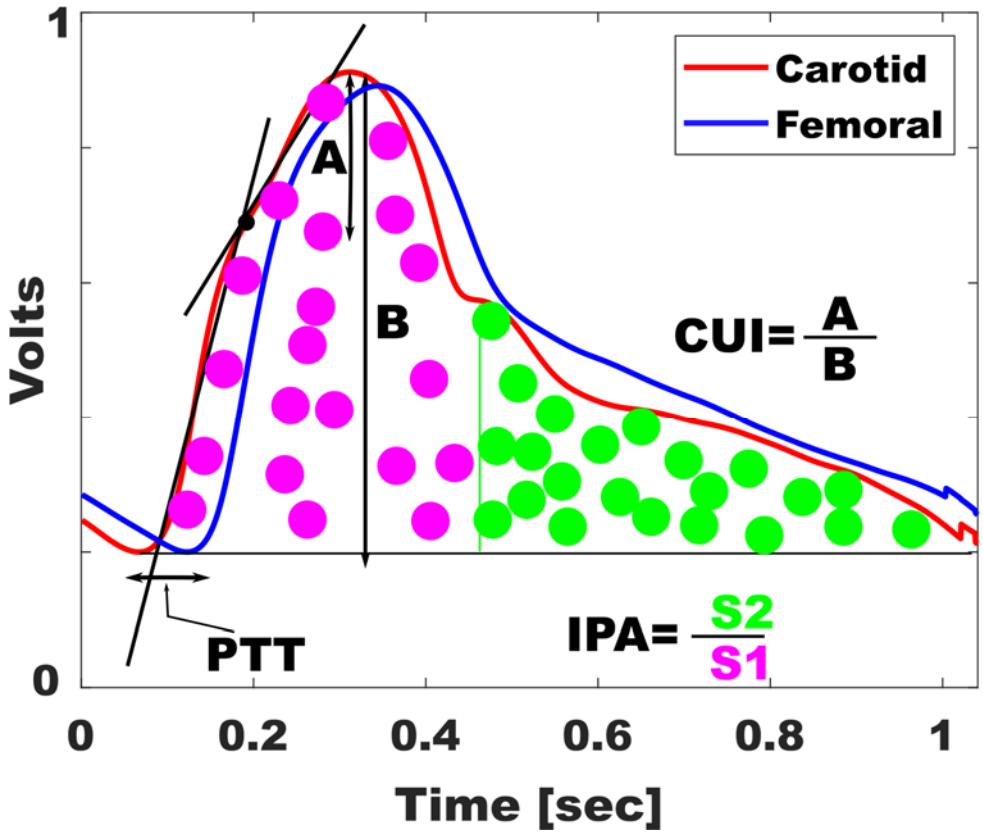

Figure 5-2 Arterial waveform features
A total of 3 features in addition to baseline features were considered as candidate for predicting the aneurysm diameter.

As also shown in the Figure 5-2, the second feature was an index obtained from two lines optimally fitted to the carotid waveform upstroke (CUI). CUI is based on the presence of an early, negative wave reflection in AAA and may increase with increasing aneurysm diameter.

Lastly, we detected a dicrotic notch and calculated the inflection point area ratio (IPA), which is the area ratio of after to before the dicrotic notch (Figure 5-2). IPA shows the strength of wave reflection. In AAA patients, due to aorta expansion, early negative wave reflection reduces the strength of the first part of the area [66].

5.2.3 Model Development and Validation

We built three linear regression models to predict abdominal aortic diameter from carotid and femoral features plus baseline features, carotid features plus baseline features, and only baseline features. We developed this model with stepwise linear regression via Stepwisefit, Matlab standard function. This function starts without features and adds or removes one feature at each step by considering statistical significance. We also applied leave-one-out cross-validation to compare the predicted and reference abdominal aortic diameters.

We used cross-correlation as the quantitative metrics of regression performance for 50 anonymized AAA patients and matched control. Furthermore, we evaluated these models in terms of their abilities to classify (i) pre- versus 3 weeks post-EVAR for 50 subjects and (ii) change from pre- to 3 weeks post-EVAR versus change from 3 weeks to 3 years post-EVAR for 17 subjects. We used receiving operating characteristics area under the curve (ROC AUC) as the quantitative metric of classification performance.

5.3 Results

50 anonymized AAA patients and 50 matched controls were used to developed linear regression models. Table 5-2 shows the results of different sets of features models in leave-one-out prediction of aneurysm diameter. All these models are robust because more than 90% of 100 models resulted in the same features. This table shows the models yielded from training on all 100 subject datasets.

Table 5-2. Regression and Classification Results. This table represents the result for the dataset, which included 50 AAA patients and 50 matched control. After finding coefficients for predicting aortic diameter, AUC (Area Under the Curve) ROC (Receiver Operating Characteristics) calculated.

Model	Coefficients	Result	AUC	CI via 1000 bootsrtap samples
Baseline	-0.02*Hr + 0.02 * Age + 6.73 * BSA	0.32	0.73	0.62-0.82
Carotid waveform plus baseline	+ 2.8*Area ratio + 0.02 * age + 4.9 * BSA	0.51	0.80	0.71-0.87
Carotid-femoral waveforms plus baseline	0.008PTT/Height*Age*DBP + 2.73* Area ratio + 0.03* weight	0.63	0.85	0.76-0.91

Baseline models, which include baseline features (see Table 5-2) resulted in a cross-correlation of 0.32 and an accuracy of 61% in classification. Adding carotid waveform features to baseline feature offered value in prediction with increasing cross-correlation to 0.51 and accuracy of 70% in classification. Using carotid and femoral waveform features plus baseline features (all the features) resulted in a cross-correlation of 0.63 and an accuracy of 85% in classification.

Table 5-3 shows the evaluation of these models in terms of their abilities to classify (i) pre- versus 3 weeks post-EVAR for 50 subjects and (ii) change from pre- to 3 weeks post-EVAR versus change from 3 weeks to 3 years post-EVAR for 17 subjects. We used receiving operating characteristics area under the curve (ROC AUC) as the quantitative metric of classification performance.

Table 5-3. Classification results for models validation. This table represents the result for the dataset, which included 50 AAA patient pre- versus 3 weeks post-EVAR patients and 17 AAA patients from 3 weeks to 3 years post-EVAR. After finding coefficients for predicting aortic diameter (see table 5-2), AUC (Area Under the Curve) ROC (Receiver Operating Characteristics) calculated. Baseline results added no value in this case.

Model	Dataset	AUC	CI via 1000 bootstrap samples
Carotid waveform plus baseline	V1 vs V2 (n=50)	0.77	0.66-0.86
	V1 -V2 vs V2-V3 (n=17)	0.92	0.76-0.98
Carotid-femoral waveforms plus baseline	V1 vs V2 (n=50)	0.78	0.68-0.86
	V1 -V2 vs V2-V3 (n=17)	0.94	0.81-0.99

The baseline model had zero value in this test because all the baseline features were the same after three weeks and three years. Carotid features showed 80% for both classification tasks. By adding femoral waveform, 90% for both classification tasks was achieved.

5.4 Discussion

An abdominal aortic aneurysm (AAA) carries increasing risk of rupture with growing diameter. This condition is often asymptomatic, so screening and surveillance are essential. Ultrasound and other imaging methods are employed for such monitoring at high accuracy. However, these methods require an expert-operator and are expensive, and AAA is considerably under-detected at present and may become even more under-detected in the future as the disease prevalence increases with societal aging. Our broad goal is to establish a device that is convenient in use and cost for AAA screening and surveillance. We hypothesize that arterial waveforms, which can be obtained with such a device, constitute a non-imaging solution for indicating aneurysm size. Here, we initially tested this hypothesis by leveraging an existing AAA patient database.

We analyzed this dataset and built a linear regression model to predict abdominal aortic diameter from features of the waveforms and patient demographic information. We considered a total of 10 baseline features and physiology-inspired waveform features. We selected the features and determined the associated regression coefficients using stepwise regression with the reference abdominal aortic diameter as the dependent variable. We also applied leave-one-out cross-validation to compare the predicted and reference abdominal aortic diameters.

Carotid and femoral waveform features yielded a good result in tracking a diameter change (Table 5-2) and in classification between AAA patients and matched control (Table 5.-2) and multiple visits (3 weeks and three years) of AAA patients (Table 5-3). All the model coefficients worked in the expected direction because increasing an aneurysm leads to increasing PTT (due to MK equation), increasing IPA (due to mismatch at the start of aortic expansion). This model suggested that a AAA monitoring device may take the form of a sensitive weighing scale to measure aortic PWV via the ballistocardiogram IJ-interval [67] in combination with a smartphone wherein the camera is placed on the neck to measure a carotid artery waveform.

Carotid waveform features yielded an acceptable result in tracking a diameter change and in classification between AAA patients and matched control (Table 5-2) and multiple visits (3 weeks and three years) of AAA patients (Table 5-3) but not as well as carotid and femoral waveform. Again, all the model coefficients worked in the expected direction. This model suggested that a AAA monitoring device may take the form of only a smartphone wherein the camera is placed on the neck to measure a carotid artery waveform. Compared to the previous model, this model is reasonably practical because it only needs a phone.

Our control group was approximately matched with AAA patients. The heart rate difference between the two groups caused the correlation coefficient of 0.32 and 70% accuracy.

In conclusion, our results demonstrate that arterial waveforms can indeed indicate AAA size. The selected waveform features suggest that a AAA monitoring device may take the form of a sensitive weighing scale to measure aortic PWV via the ballistocardiogram IJ-interval [67] in combination with a smartphone wherein the camera is placed on the neck to measure a carotid artery waveform. Such a convenient, non-imaging device could be more effective than aortic palpation in indicating if an ultrasound scan is needed.

Chapter 6. Conclusion and Future Work

The first part of this thesis concludes a series of studies on PTT/PPG for cuffless BP. In the first step, we showed that toe PAT is by far best compared to conventional PTTs. In the second step, we showed that adding PPG features can help ear and finger locations, but toe PAT is still a bit better on average. In the third step, we showed that the toe PAT model is valid longer than other models and at least a year. Taken together, this trio of studies supports toe PAT for cuffless BP.

This conclusion suggests that it may be necessary to obtain innovative PTTs to improve the correlation with BP via novel sensors and/or waveform detections. Innovative sensors may include ballistocardiography [67], seismocardiography [68], wrist bioimpedance [50], ultrasound, and radar sensors.

The second part of this thesis suggests that an AAA monitoring device may take the form of a sensitive weighing scale to measure aortic PWV via the ballistocardiogram IJ-interval [67] or a smartphone (Figure 6-1) wherein the camera is placed on the neck to measure a carotid artery waveform. Such a convenient, non-imaging device could be more effective than aortic palpation in indicating whether an ultrasound scan is needed or not.

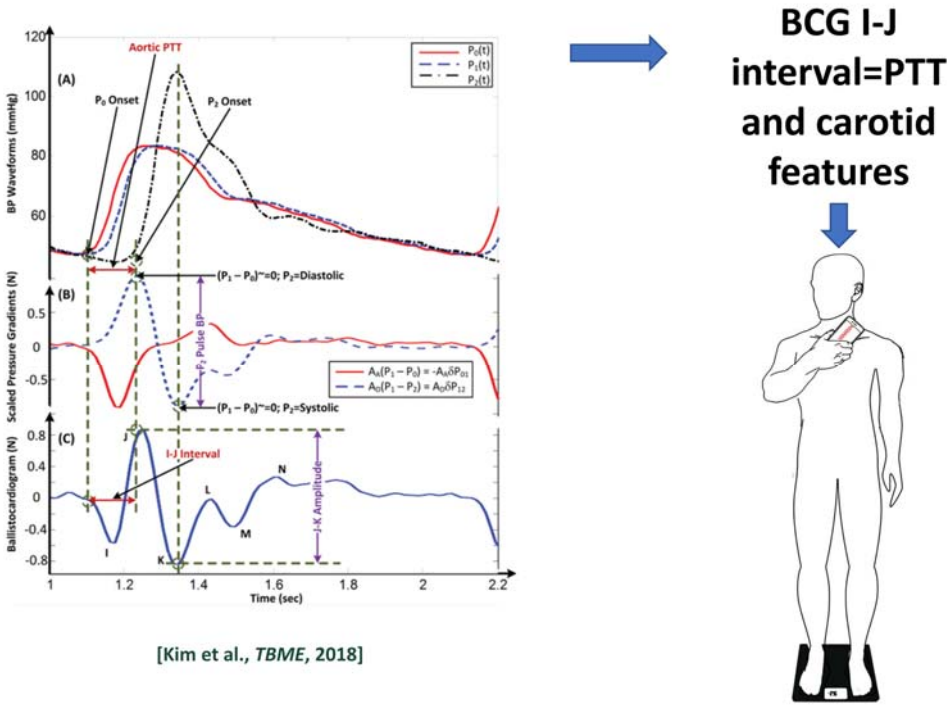

Figure 6-1 Screening and surveillance of AAA with arterial waveforms.

BIBIOGRAPHY

BIBLIOGRAPHY

[1] C. Bramwell and A. V Hill, "The velocity of pulse wave in man," *Proc. R. Soc. London. Ser. B*, vol. 93, no. 652, pp. 298–306, 1922.

[2] R. Mukkamala, J.-O. Hahn, O. T. Inan, L. K. Mestha, C.-S. Kim, H. Toreyin, and S. Kyal, "Toward ubiquitous blood pressure monitoring via pulse transit time: theory and practice," *IEEE Trans. Biomed. Eng.*, vol. 62, no. 8, pp. 1879–1901, 2015.

[3] R. Asmar, A. Benetos, J. Topouchian, P. Laurent, B. Pannier, A.-M. Brisac, R. Target, and B. I. Levy, "Assessment of arterial distensibility by automatic Pulse Wave Velocity measurement," *Hypertension*, vol. 26, no. 3, pp. 485–490, Sep. 1995.

[4] K. H. Parker, "A brief history of arterial wave mechanics," *Med. Biol. Eng. Comput.*, vol. 47, no. 2, pp. 111–118, 2009.

[5] C. Vlachopoulos, M. O'Rourke, and W. Nichols, *McDonald's blood flow in arteries: theoretical, experimental and clinical principles*. London: CRC press, 2011.

[6] F. U. S. Mattace-Raso, A. Hofman, G. C. Verwoert, J. C. M. Wittemana, I. Wilkinson, J. Cockcroft, C. McEniery, Yasmina, S. Laurent, P. Boutouyrie, E. Bozec, T. W. Hansen, C. Torp-Pedersen, H. Ibsen, J. Jeppesen, S. J. Vermeersch, E. Rietzschel, M. de Buyzere, T. C. Gillebert, L. van Bortel, P. Segers, C. Vlachopoulos, C. Aznaouridis, C. Stefanadis, A. Benetos, C. Labat, P. Lacolley, C. D. A. Stehouwer, G. Nijpels, J. M. Dekker, I. Ferreira, J. W. R. Twisk, S. Czernichow, P. Galan, S. Hercberg, B. Pannier, A. Guérin, G. London, J. Kennedy Cruickshank, S. G. Anderson, A. Paini, E. A. Rosei, M. L. Muiesan, M. Salvetti, J. Filipovsky, J. Seidlerova, and M. Dolejsova, "Determinants of pulse wave velocity in healthy people and in the presence of cardiovascular risk factors: 'Establishing normal and reference values,'" *Eur. Heart J.*, vol. 31, no. 19, pp. 2338–2350, 2010.

[7] H. U. Chung, B. H. Kim, J. Y. Lee, J. Lee, Z. Xie, E. M. Ibler, K. H. Lee, A. Banks, J. Y. Jeong, J. Kim, C. Ogle, D. Grande, Y. Yu, H. Jang, P. Assem, D. Ryu, J. W. Kwak, M. Namkoong, J. Bin Park, Y. Lee, D. H. Kim, A. Ryu, J. Jeong, K. You, B. Ji, Z. Liu, Q. Huo, X. Feng, Y. Deng, Y. Xu, K. I. Jang, J. Kim, Y. Zhang, R. Ghaffari, C. M. Rand, M. Schau, A. Hamvas, D. E. Weese-Mayer, Y. Huang, S. M. Lee, C. H. Lee, N. R. Shanbhag, A. S. Paller, S. Xu, and J. A. Rogers, "Binodal, wireless epidermal electronic systems with in-sensor analytics for neonatal intensive care," *Science (80-.).*, vol. 363, no. 6430, p. eaau0780, 2019.

[8] C. Wang, X. Li, H. Hu, L. Zhang, Z. Huang, M. Lin, Z. Zhang, Z. Yin, B. Huang, H. Gong, S. Bhaskaran, Y. Gu, M. Makihata, Y. Guo, Y. Lei, Y. Chen, C. Wang, Y. Li, T. Zhang, Z. Chen, A. P. Pisano, L. Zhang, Q. Zhou, and S. Xu, "Monitoring of the central blood pressure waveform via a conformal ultrasonic device," *Nat. Biomed. Eng.*, vol. 2, no. 9, pp. 687–695, 2018.

[9] W. F. Hamilton, W. Remington, and P. Dow, "The determination of the propagation velocity of the arterial pulse wave," *Am. J. Physiol.*, vol. 144, no. 4, pp. 521–535, 1945.

[10] G. Klug, H. Feistritzer, S. Reinstadler, A. Mayr, C. Kremser, M. Schocke, W. Franz, and M. B, "Use and limitations of cardiac magnetic resonance derived measures of aortic stiffness in patients after acute myocardial infarction," *Magn. Reson. Imaging*, vol. 32, no. 10, pp. 1259–1265, 2014.

[11] A. Harloff, H. Mirzaee, T. Lodemann, P. Hagenlocher, T. Wehrum, J. Stuplich, A. Hennemuth, J. Hennig, S. Grundmann, and W. Vach, "Determination of aortic stiffness using 4D flow cardiovascular magnetic resonance - A population-based study," *J. Cardiovasc. Magn. Reson.*, vol. 20, no. 1, 2018.

[12] J. J. M. Westenberg, E. P. Van Poelgeest, P. Steendijk, H. B. Grotenhuis, J. W. Jukema, and A. De Roos, "Bramwell-Hill modeling for local aortic pulse wave velocity estimation: A validation study with velocity-encoded cardiovascular magnetic resonance and invasive pressure assessment," *J. Cardiovasc. Magn. Reson.*, vol. 14, no. 1, pp. 1–10, 2012.

[13] J. W. Remington and W. F. Hamilton, "The construction of a theoretical cardiac ejection curve from the contour of the aortic pressure pulse," *Am. J. Physiol. Content*, vol. 144, no. 4, pp. 546–556, 1945.

[14] B. P. Hallock and I. C. Benson, "Studies on the elastic properties of human isolated aorta," *J. Clin. Invest.*, vol. 16, no. 4, pp. 595–602, 1937.

[15] A. L. King, "Circulatory System: Arterial Pulse; Wave velocity," *Med. Phys.*, vol. 2, no. 1, pp. 188–191, 1950.

[16] A. Moens, *Die Pulscurve*. Leiden: The Netherlands: Bril, 1878.

[17] Ye Li, "Propagation and reflection of pulse wave in flexible tubes and relation to wall properties [PhD thesis]," Brunel University, 2011.

[18] S. Graf, D. Craiem, M. Valero, M. Alfonso, J. G. Barra, and R. L. Armentano, "Mechanical properties of the aortic arterial wall during 24 hours: A preliminary study in conscious sheep," *J. Phys. Conf. Ser.*, vol. 332, no. 1, p. 012008, 2011.

[19] H. J. Feistritzer, S. J. Reinstadler, G. Klug, C. Kremser, B. Seidner, R. Esterhammer, M. F. Schocke, W. M. Franz, and B. Metzler, "Comparison of an oscillometric method with cardiac magnetic resonance for the analysis of aortic pulse wave velocity," *PLoS One*, vol. 10, no. 1, 2015.

[20] H. J. Feistritzer, G. Klug, S. J. Reinstadler, M. Reindl, L. Niess, T. Nalbach, C. Kremser, A. Mayr, and B. Metzler, "Prognostic value of aortic stiffness in patients after ST-elevation myocardial infarction," *J. Am. Heart Assoc.*, vol. 6, no. 9, p. e005590, 2017.

[21] J. W. Remington, W. F. Hamilton, and P. Dow, "Some difficulties involved in the prediction of the stroke volume from the pulse wave velocity," *Am. J. Physiol. Content*, vol. 144, no. 4, pp. 536–545, 1945.

[22] I. Tan, M. Butlin, B. Spronck, H. Xiao, and A. Avolio, “Effect of heart rate on arterial stiffness as assessed by pulse wave velocity,” *Curr. Hypertens. Rev.*, vol. 14, no. 2, pp. 107–122, 2017.

[23] D. H. Bergel, “The visco-elastic properties of the arterial wall [PhD thesis],” University of London, 1960.

[24] F. J. Callaghan, C. F. Babbs, J. D. Bourland, and L. A. Geddes, “The relationship between arterial pulse-wave velocity and pulse frequency at different pressures,” *J. Med. Eng. Technol.*, vol. 8, no. 1, pp. 15–18, 1984.

[25] Y. C. Gao, “Asymptotic analysis of the nonlinear Boussinesq problem for a kind of incompressible rubber material (compression case),” *J. Elast.*, vol. 64, no. 2, pp. 111–130, 2001.

[26] D. Carnelli, A. Karimi, and J. P. Franc, “Application of spherical nanoindentation to determine the pressure of cavitation impacts from pitting tests,” *J. Mater. Res.*, vol. 27, no. ARTICLE, pp. 91–99, 2012.

[27] R. Berne and M. Levy, *Cardiovascular physiology*, 4th ed. Mosby, 1981.

[28] M. Roger G, “Physiological fluid mechanics,” in *Lecture notes*, MASSACHUSETTS INSTITUTE OF TECHNOLOGY, 2003.

[29] Y.-C. Fung, *Biomechanics: Circulation*. Springer, 1997.

[30] G. J. Langewouters, K. H. Wesseling, and W. J. A. Goedhard, “The static elastic properties of 45 human thoracic and 20 abdominal aortas in vitro and the parameters of a new model,” *J. Biomech.*, vol. 17, no. 6, pp. 425–435, 1984.

[31] M. Yavarimanesh, A. Chandrasekhar, J. O. Hahn, and R. Mukkamala, “Commentary: Relation between blood pressure and pulse wave velocity for human arteries,” *Front. Physiol.*, vol. 10, no. 1, pp. 1179–1181, 2019.

[32] K. H. Parker, “An introduction to wave intensity analysis,” *Med. Biol. Eng. Comput.*, vol. 47, no. 2, pp. 175–188, 2009.

[33] J. Solà and R. Delgado-Gonzalo, *The Handbook of Cuffless Blood Pressure Monitoring*. Cham: Springer International Publishing, 2019.

[34] M. Radha, G. Zhang, J. Gelissen, K. De Groot, R. Hakkma, and R. Aarts, “Arterial path selection to measure pulse wave velocity as a surrogate marker of blood pressure,” *Biomed. Phys. Eng. Express*, vol. 3, no. 1, p. 015022, 2017.

[35] S. Rajala, H. Lindholm, and T. Taipalus, “Comparison of photoplethysmogram measured from wrist and finger and the effect of measurement location on pulse arrival time,” *Physiol. Meas.*, vol. 39, no. 7, p. 075010, 2018.

[36] J. Lee, S. Yang, S. Lee, and H. Kim, "Analysis of pulse arrival time as an indicator of blood pressure in a large surgical biosignal database: recommendations for developing ubiquitous blood," *J. Clin. Med.*, vol. 8, no. 11, p. 1773, 2019.

[37] W. Chen, T. Kobayashi, S. Ichikawa, Y. Takeuchi, and T. Togawa, "Continuous estimation of systolic blood pressure using the pulse arrival time and intermittent calibration," *Med. Biol. Eng. Comput.*, vol. 38, no. 5, pp. 569–574, Sep. 2000.

[38] B. Escobar-Restrepo, R. Torres-Villa, and P. A. Kyriacou, "Evaluation of the linear relationship between pulse arrival time and blood pressure in ICU patients: potential and limitations," *Front. Physiol.*, vol. 9, p. 1848, 2018.

[39] M. Gao, N. B. Olivier, and R. Mukkamala, "Comparison of noninvasive pulse transit time estimates as markers of blood pressure using invasive pulse transit time measurements as a reference," *Physiol. Rep.*, vol. 4, no. 10, pp. 1–7, 2016.

[40] R. A. Payne, C. N. Symeonides, D. J. Webb, and S. R. J. Maxwell, "Pulse transit time measured from the ECG: an unreliable marker of beat-to-beat blood pressure," *J. Appl. Physiol.*, vol. 100, no. 1, pp. 136–141, 2006.

[41] Y. Chen, C. Wen, G. Tao, M. Bi, and G. Li, "Continuous and noninvasive blood pressure measurement : a novel modeling methodology of the relationship between blood pressure and pulse wave velocity," *Ann. Biomed. Eng.*, vol. 37, no. 11, pp. 2222–2233, 2009.

[42] C. N. Joseph, C. Porta, G. Casucci, N. Casiraghi, M. Maffeis, M. Rossi, and L. Bernardi, "Slow breathing improves arterial baroreflex sensitivity and decreases blood pressure in essential hypertension," *Hypertension*, vol. 46, no. 4, pp. 714–718, 2005.

[43] M. Al'Absi, S. Bongard, T. Buchanan, G. Pincomb, J. Lincino, and W. Lovallo, "Cardiovascular and neuroendocrine adjustment to public speaking and mental arithmetic stressors," *Psychophysiology*, vol. 34, no. 3, pp. 266–275, 1997.

[44] E. A. Hines and G. E. Brown, "The cold pressor test for measuring the reactibility of the blood pressure: Data concerning 571 normal and hypertensive subjects," *Am. Heart J.*, vol. 11, no. 1, pp. 1–9, Jan. 1936.

[45] M. Gao, H.-M. Cheng, S.-H. Sung, C.-H. Chen, N. B. Olivier, and R. Mukkamala, "Estimation of pulse transit time as a function of blood pressure using a nonlinear arterial tube-load model," *IEEE Trans. Biomed. Eng.*, vol. 64, no. 7, pp. 1524–1534, 2017.

[46] A. Chandrasekhar, M. Yavarimanesh, K. Natarajan, J. Hahn, and R. Mukkamala, "PPG sensor contact pressure should be taken into account for cuff-less blood pressure measurement," *IEEE Trans. Biomed. Eng.*, 2020.

[47] C.-S. Kim, A. M. Carek, O. Inan, R. Mukkamala, and J.-O. Hahn, "Ballistocardiogram-based approach to cuff-less blood pressure monitoring: proof-of-concept and potential challenges," *IEEE Trans. Biomed. Eng.*, vol. 65, no. 11, pp. 2384–2391, 2018.

[48] M. Di Rienzo, E. Vaini, and P. Lombardi, “Use of seismocardiogram for the beat-to-beat assessment of the pulse transit time: a pilot study,” in *2015 37th Annual International Conference of the IEEE Engineering in Medicine and Biology Society (EMBC)*, 2015, vol. 2015, pp. 7184–7187.

[49] C. Yang and N. Tavassolian, “Pulse transit time measurement using seismocardiogram, photoplethysmogram, and acoustic recordings: evaluation and comparison,” *IEEE J. Biomed. Heal. Informatics*, vol. 22, no. 3, pp. 733–740, 2018.

[50] B. Ibrahim and R. Jafari, “Cuffless blood pressure monitoring from an array of wrist bio-impedance sensors using subject-specific regression models: proof of concept,” *IEEE Trans. Biomed. Circuits Syst.*, 2019.

[51] P. M. Nabeel, J. Joseph, S. Karthik, M. Sivaprakasam, and M. Chenniappan, “Bi-modal arterial compliance probe for calibration-free cuffless blood pressure estimation,” *IEEE Trans. Biomed. Eng.*, vol. 65, no. 11, pp. 2392–2404, 2018.

[52] D. Buxi, J.-M. Redout, and M. R. Yuce, “Blood pressure estimation using pulse transit time from bioimpedance and continuous wave radar,” *IEEE Trans. Biomed. Eng.*, vol. 64, no. 4, pp. 917–927, Apr. 2017.

[53] D. Xu, K. L. Ryan, C. A. Rickards, G. Zhang, V. A. Convertino, and R. Mukkamala, “Improved pulse transit time estimation by system identification analysis of proximal and distal arterial waveforms,” *Am. J. Physiol. Circ. Physiol.*, vol. 301, no. 4, pp. H1389–H1395, 2011.

[54] Z. Ghasemi, J. Lee, C. Kim, H. Cheng, S. Sung, C. Chen, R. Mukkamala, and J. Hahn, “Estimation of cardiovascular risk predictors from non-invasively measured diametric pulse volume waveforms via multiple measurement information fusion,” *Sci. reports* , vol. 8, no. 1, p. 10433, 2018.

[55] W. MY, P. CC, and Z. YT, “An evaluation of the cuffless blood pressure estimation based on pulse transit time technique: a half year study on normotensive subjects,” *Cardiovasc. Eng.*, vol. 9, no. 1, pp. 32–38, 2009.

[56] R. Block, M. Yavarimanesh, K. Natarajan, A. Carek, A. Mousavi, A. Chandrasekhar, C. Kim, J. Zhu, G. Schifitto, L. Mestha, O. Inan, and R. Mukkamala, “Conventional pulse transit times as markers of blood pressure changes in humans,” *Sci. Reports* , vol. 10, no. 1, pp. 1–9, 2020.

[57] R. Mukkamala and J. Hahn, “Toward ubiquitous blood pressure monitoring via pulse transit time: Predictions on maximum calibration period and acceptable error limits,” *IEEE Trans. Biomed. Eng.*, vol. 65, no. 6, pp. 1410–1420, 2017.

[58] K. Natarajan, R. Block, M. Yavarimanesh, A. Chandrasekhar, L. Mestha, O. Inan, J. Hahn, and R. Mukkamala, “Photoplethysmography fast upstroke time intervals can be useful features for cuff-less measurement of blood pressure changes in humans,” *IEEE Trans. Biomed. Eng.*, vol. 1, no. 1, pp. 1–9, 2021.

[59] M. L. LeFevre, “Screening for abdominal aortic aneurysm: U.S. preventive services task force recommendation statement,” *Ann. Intern. Med.*, vol. 161, no. 4, pp. 281–290, 2014.

[60] S. Aggarwal, A. Qamar, V. Sharma, and A. Sharma, “Abdominal aortic aneurysm: A comprehensive review,” *Exp. Clin. Cardiol.*, vol. 16, no. 1, p. 11, 2011.

[61] G. A. Kuzmik, A. X. Sang, and J. A. Elefteriades, “Natural history of thoracic aortic aneurysms,” *J. Vasc. Surg.*, vol. 55, no. 2, pp. 565–571, 2012.

[62] F. A. Lederle, “The rise and fall of abdominal aortic aneurysm,” *Circulation*, vol. 124, no. 10, pp. 1097–1099, 2011.

[63] J. Chung, “Epidemiology, risk factors, pathogenesis, and natural history of abdominal aortic aneurysm,” *UpToDate*, 2019.

[64] Smith-Burgess L, “Early identification and detection of abdominal aortic aneurysms | Clinical | Nursing Times,” *Nursing Times*, 2017.

[65] C. W. Lee, S. H. Sung, C. K. Chen, I. M. Chen, H. M. Cheng, W. C. Yu, C. C. Shih, and C. H. Chen, “Measures of carotid-femoral pulse wave velocity and augmentation index are not reliable in patients with abdominal aortic aneurysm,” *J. Hypertens.*, vol. 31, no. 9, pp. 1853–1860, 2013.

[66] L. Wang, E. Pickwell-MacPherson, Y. P. Liang, and Y. T. Zhang, “Noninvasive cardiac output estimation using a novel photoplethysmogram index,” *2009 Annu. Int. Conf. IEEE Eng. Med. Biol. Soc.*, 2009.

[67] C. S. Kim, S. L. Ober, M. S. McMurtry, B. A. Finegan, O. T. Inan, R. Mukkamala, and J. O. Hahn, “Ballistocardiogram: mechanism and potential for unobtrusive cardiovascular health monitoring,” *Sci. Rep.*, vol. 6, no. 1, p. 31297, 2016.

[68] O. T. Inan, P.-F. Migeotte, K.-S. Park, M. Etemadi, K. Tavakolian, R. Casanella, J. Zanetti, J. Tank, I. Funtova, G. K. Prisk, and M. Di Rienzo, “Ballistocardiography and seismocardiography: a review of recent advances,” *IEEE J. Biomed. Heal. Informatics*, vol. 19, no. 4, pp. 1414–1427, 2015.